Soft Matter

PAPER

Cite this: *Soft Matter*, 2019, **15**, 1758

Electroadhesion with application to touchscreens

Omer Sirin,[a] Mehmet Ayyildiz,[bc] B. N. J. Persson[b] and Cagatay Basdogan*[a]

Received 29th November 2018,
Accepted 11th January 2019

DOI: 10.1039/c8sm02420k

rsc.li/soft-matter-journal

There is growing interest in touchscreens displaying tactile feedback due to their tremendous potential in consumer electronics. In these systems, the friction between the user's fingerpad and the surface of the touchscreen is modulated to display tactile effects. One of the promising techniques used in this regard is electrostatic actuation. If, for example, an alternating voltage is applied to the conductive layer of a surface capacitive touchscreen, an attractive electrostatic force is generated between the finger and the surface, which results in an increase in frictional forces acting on the finger moving on the surface. By altering the amplitude, frequency, and waveform of this signal, a rich set of tactile effects can be generated on the touchscreen. Despite the ease of implementation and its powerful effect on our tactile sensation, the contact mechanics leading to an increase in friction due to electroadhesion has not been fully understood yet. In this paper, we present experimental results for how the friction between a finger and a touchscreen depends on the electrostatic attraction and the applied normal pressure. The dependency of the finger–touchscreen interaction on the applied voltage and on several other parameters is also investigated using a mean field theory based on multiscale contact mechanics. We present detailed theoretical analysis of how the area of real contact and the friction force depend on contact parameters, and show that it is possible to further augment the friction force, and hence the tactile feedback displayed to the user by carefully choosing those parameters.

1 Introduction

A touchscreen, a display screen that is sensitive to the touch of a finger or stylus, has been available for nearly half a century. It has been widely used on ATM machines, retail point-of-sale terminals, game consoles, car navigation systems, medical monitors, and industrial control panels. After the introduction of touchscreen-based mobile devices in the late 2000s, the capacitive touchscreen has become widely popular on hand-held devices such as personal computers, tablets, personal digital assistants, smart watches, and e-book readers. Today, the touchscreen is one of the easiest to use and most intuitive of all computer interfaces, which allows users to naturally and directly interact with what is displayed (text, pictures and other data), rather than using a traditional keyboard or mouse. One important effort to make this interaction more powerful is to provide effective, feasible and inexpensive tactile feedback to the user. In this regard, two leading surface haptic technologies have emerged during the last few years. One is based on the modulation of friction between a human fingertip and an active surface through electroadhesion.[1–5] The other involves ultrasonic vibrations to reduce the friction, and generate a squeeze film effect (creating a thin cushion of air) between the fingertip and the counter surface.[6,7]

The electrical attraction between a charged surface and human skin was discovered by Johnsen and Rahbek[8] in 1923. Later, in 1953 Mallinckrodt[9] reported an increase in the friction during touch when an alternating voltage is applied to an insulated aluminum plate. He observed that the input voltage signal creates an alternating electrostatic force that periodically attracts and releases the finger from the surface, producing friction-like rubbery sensations when the finger moves on the surface. This effect has recently been intensively studied, *e.g.*, for grippers for robotics,[10–12] and in the context of mobile touchscreens.[13,14] In particular, the potential applications of touchscreens displaying tactile feedback in education, games, communication, data visualization, and user interface development for blind people are highly promising.

When an alternating electric potential is applied to the conductive layer of a touchscreen, the insulating layer on the glass plate and the finger are polarized by induction (*i.e.*, charges of opposite sign are accumulated on the surfaces at the contacting interface). Thus, an electrostatic attraction force due to "electroadhesion" is generated between the finger and the counter surface in the normal direction, which increases the sliding friction between the finger and the glass plate. This phenomenon was

[a] *College of Engineering, Koc University, Istanbul, Turkey. E-mail: cbasdogan@ku.edu.tr*
[b] *PGI-1, FZ Jülich, Germany. Web: www.MultiscaleConsulting.com*
[c] *Faculty of Engineering and Natural Sciences, Istanbul Bilgi University, Istanbul, Turkey*

referred to as "electrovibration" by Grimnes,[15] who also reported that the generated tactile sensation depends on the roughness and moisture of the finger.

Human skin is highly sensitive to variations in friction force. The nature of the contact interface and involved materials (*e.g.*, surface topographies, contamination films, and atomic and molecular characteristics) strongly influences the sliding friction,[16–18] in addition to external conditions such as temperature, humidity, mechanical vibrations and electric fields. For example, the friction force generated by the electrostatic attraction depends on the frequency, waveform and amplitude of the applied electric potential.[2,5,19] A rich set of tactile effects can be potentially generated by varying these parameters.[4] In spite of the ease of implementation and its powerful effect on our tactile sensation, the contact mechanics leading to an increase in friction due to electroadhesion has not been fully understood yet.

In this paper, we present theoretical and experimental results for the estimation of the friction resulting from the electrostatic attraction between the human finger and a touchscreen. The dependency of the finger–touchscreen interaction on the applied voltage, and on several other contact parameters, was investigated using a mean field theory based on multiscale contact mechanics. For the experimental measurements, a tribometer was developed to move the index finger of an experimenter back and forth on the touchscreen using a motorized slider. The friction force at a sliding speed of $v = 50$ mm s^{-1} was recorded as a function of the normal force, varied incrementally from 0.2 N to 2 N. The amplitude of the voltage signal applied to the conductive layer of the touchscreen at 125 Hz was varied between $V_0 = 0$ V and $V_0 = 200$ V (with an increment of 25 V). The experimental results were compared to those produced by the theory. Also, the dependency of the electroadhesion friction on the frequency of the oscillating electric potential was investigated using the proposed theory. Finally, a discussion on the origin and enhancement of the friction due to electroadhesion is provided, along with the corresponding design criteria, and the limitations of the study and the challenges ahead are also discussed.

2 Theory: a mean field model for electroadhesion

Fig. 1 shows an elastic solid having a multi-scale surface roughness above a rigid solid having a flat and smooth surface. Both solids are conducting materials with insulating surface layers of thicknesses d_1 and d_2 and dielectric constants ε_1 and ε_2. We define the effective insulator thickness as $h_0 = d_1/\varepsilon_1 + d_2/\varepsilon_2$. The interfacial separation $u = u(\mathbf{x})$ between the solids depends on the lateral coordinate $\mathbf{x} = (x,y)$.

The solids make atomic contact in a fraction A/A_0 of the nominal contact area A_0 (in the figure $A = 0$). The non-contact regions are filled with air but we can consider these regions as vacuum because the (relative) dielectric constant of air ($\varepsilon_{air} \approx 1.00059$) is nearly the same as that of vacuum ($\varepsilon = 1$).

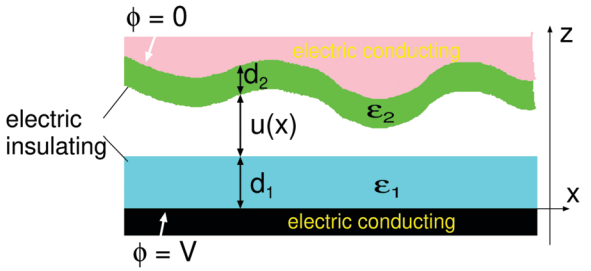

Fig. 1 An elastic solid with surface roughness above a rigid solid with a flat surface. Both solids are conducting materials with insulating surface layers of thicknesses d_1 and d_2 and dielectric constants ε_1 and ε_2. An electric voltage difference V occurs between the two conducting solids. The interfacial separation $u = u(\mathbf{x})$ depends on the lateral coordinate $\mathbf{x} = (x,y)$.

Assume now that an electric potential $\phi(t) = V_0\cos(\omega_0 t)$ is applied between the solids as indicated in Fig. 1. This will give rise to an electric field in the air-gap between the solids, which results in an attractive force that can be calculated from the zz-component of the Maxwell stress tensor:[20]

$$\sigma_{zz} = \frac{1}{2}\varepsilon_0 E_z^2, \tag{1}$$

where ε_0 is the dielectric function of vacuum. The electric field at the bottom surface of the upper solid (the SC–air interface) is:[20]

$$E_z = -\mathrm{Re}\left[\frac{V_0 e^{-i\omega_0 t}}{u + h_0(\omega)}\right]. \tag{2}$$

The normal stress averaged over the surface roughness becomes

$$\langle\sigma_{zz}\rangle = \frac{1}{4}\varepsilon_0 V_0^2 \int_0^\infty du\, P(p,u)\frac{1+\cos(2\omega_0 t + 2\phi)}{|u + h_0(\omega_0)|^2}, \tag{3}$$

where $P(p,u)$ is the probability distribution for the interfacial separation u, which depends on the squeezing pressure p (see below).

Assume that we squeeze the upper solid against the substrate with a force F_0. When an electric potential is applied between the solids, there will be an additional electric force acting on them. In the simplest approach, one includes the electric attraction $p_a = \langle\sigma_{zz}\rangle$ as a contribution to the external load. Thus we write the effective squeezing or loading pressure as

$$p = p_0 + p_a, \tag{4}$$

where $p_0 = F_0/A_0$ is the applied pressure. Intuitively, one expects this approach to be accurate when the interaction force between the surfaces is long-range. A similar approach has also been successfully used for modeling the attraction resulting from capillary bridges.[21,22]

To calculate $p_a = \langle\sigma_{zz}\rangle$, we need to know the probability distribution $P(p,u)$. For randomly rough surfaces, the function $P(p,u)$ has been approximately calculated.[23,24] Using eqn (3) and (4), the time (and space) average of the effective pressure is obtained as

$$p = p_0 + \frac{1}{4}\varepsilon_0 V_0^2 \int_0^\infty du\, P(p,u)\frac{1}{|u + h_0|^2}. \tag{5}$$

The electric potential can be calculated from the above equation as

$$V_0^2 = \frac{4(p - p_0)/\varepsilon_0}{\int_0^\infty \mathrm{d}u\ P(p,u)|u + h_0|^{-2}}. \quad (6)$$

For a homogeneous elastic solid, the relative contact area A/A_0 can be obtained by using[25]

$$\frac{A}{A_0} \approx \frac{\sqrt{\pi}}{2}\mathrm{erf}\left(\frac{2p}{h'E^*}\right), \quad (7)$$

where h' is the rms slope of the combined surface roughness profile and $E^* = E/(1 - \nu^2)$ (where E and ν are the Young's modulus and Poisson ratio of the elastic solid, respectively). This equation is valid for the contact between homogeneous elastic solids with random surface roughness. When $A/A_0 \ll 1$, eqn (7) reduces to

$$\frac{A}{A_0} \approx \frac{2p}{h'E^*}. \quad (8)$$

Human skin is a layered material and hence h' is not the rms-slope of the combined surface roughness, but a quantity which depends on the surface roughness power spectrum as well as the elastic moduli and thicknesses of the layers.[26] In addition, for dry skin, the local contact pressures are typically so large that plastic deformation may occur, and in this case one cannot use eqn (7) or (8) directly to calculate the contact area but the full theory described elsewhere[25,26] must be used.

From the knowledge of A, we obtain the friction force from

$$F_f = A\tau_f. \quad (9)$$

The frictional shear stress τ_f is independent of the asperity contact pressure $p^* = pA_0/A$ as long as p^* is less than a few MPa. As an example, which is of interest for grippers in robotics applications, for silicone rubber (PDMS) sliding (in complete contact) on a smooth glass surface with a speed of $v \approx 1$ mm s^{-1}, the experiments have shown that $\tau_f \approx 0.1$ MPa.[27] At the same sliding speed, for other types of rubber $\tau_f \approx$ 1–10 MPa,[28,29] and for human skin, which is of interest for touchscreens, $\tau_f = 5$–13 MPa.[30,31] This is also similar to what is observed for plastics (polymers below the glass transition temperature).[32]

We note that electroadhesion for dry finger skin depends on what is called the finite size effect (see Appendix A), and that adhesion exists even if the solids are rigid. When finite size effects are important, one expects the contact area A to depend on the nominal contact pressure p_0 (for small contact pressures) as shown in Fig. 2 (blue curve). Note that the contact area curve $A(p_0)$ with adhesion when finite size effects are important (blue curve) is nearly parallel to the one without the adhesion (black curve). This differs drastically from the case where finite size effects are negligible and the change in the contact area as a function of load (for small applied loads) has the form shown with the green line in Fig. 2. In this case, the slope of the $A(p_0)$ line is much bigger than when finite size effects are important. Our experiments and the theoretical analysis show that finite size effects can be important for the dry finger skin having a high elastic modulus of the SC, E_{SC}.

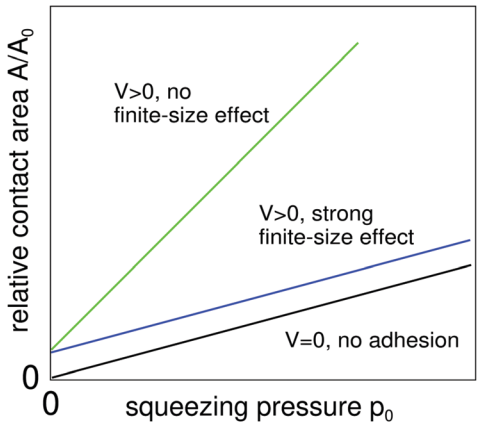

Fig. 2 The relative contact area as a function of the squeezing pressure without adhesion (black line), with adhesion for a system with a negligible finite-size effect (green line), and for a system with a strong finite-size effect (blue line).

2.1 Comparison with earlier studies

Let us compare our basic formula for the electroadhesion pressure with what have been used before. First, using eqn (3) and the definition of effective insulator layer thickness, we obtain

$$p_a = \frac{1}{4}\varepsilon_0 V_0^2 \int_0^\infty \mathrm{d}u\ P(p,u)\frac{1 + \cos(2\omega_0 t + \phi)}{|u + d_1/\varepsilon_1 + d_2/\varepsilon_2|^2}. \quad (10)$$

If we assume that the air-film has a uniform thickness $\bar{u}$, then the probability distribution becomes $P(p,u) = \delta(u - \bar{u})$ and the time average of eqn (10) takes the form

$$p_a = \frac{1}{4}\frac{\varepsilon_0 V_0^2}{|\bar{u} + d_1/\varepsilon_1 + d_2/\varepsilon_2|^2}. \quad (11)$$

If we also assume that the dielectric functions $\varepsilon_1(\omega_0)$ and $\varepsilon_2(\omega_0)$ are real, then we get

$$p_a = \frac{1}{4}\frac{\varepsilon_0 V_0^2}{(\bar{u} + d_1/\varepsilon_1 + d_2/\varepsilon_2)^2}. \quad (12)$$

This equation has been used in earlier studies to calculate the electroadhesive force per unit surface area.[33] However, it would be valid only if (a) the air film would have uniform thickness $\bar{u}$ and (b) the dielectric functions of the SC and the insulating layer would be real. Assumption (b) is a reasonable one in most cases of interest, but assumption (a) is a poor one when the average thickness of the air gap (determined mainly by the surface roughness of the SC) $\bar{u} \approx 10$ μm is much larger than the effective thickness $h_0 = d_1/\varepsilon_1 + d_2/\varepsilon_2 \approx 0.3$ μm. The reason for this is that in expression (10) the most important contribution arises when u is small, *i.e.*, from the areas of real contacts and from the so called rim-areas which are narrow strips of non-contact areas around the contact regions where the surface separation $u(\mathbf{x})$ is very small.

Assumption (b) breaks down when the electrical conductivity of the SC (or of the insulating glass film) becomes

important, which is the case at very low frequency ω. For low frequencies, the dielectric function of the SC is of the form

$$\varepsilon = \varepsilon_{SC} + \frac{i}{\omega\varepsilon_0\rho_{SC}}, \tag{13}$$

where $\rho_{SC}(\omega)$ is the (frequency-dependent) electrical resistivity of the skin SC (see Fig. 7). Note that when $1/(\omega\varepsilon_0\rho_{SC}) > \varepsilon_{SC}$ or $\omega < 1/(\varepsilon_0\varepsilon_{SC}\rho_{SC})$, the SC will act like a conducting layer, and the mobile charges in the skin will be located at the skin surface rather than at the interface between the SC and the underlying tissue of the skin. Measurements[34] for the dry human skin have shown that both ε_{SC} and ρ_{SC} depend on the frequency and that $1/(\omega\varepsilon_0\rho_{SC}) > \varepsilon_{SC}$ for $\omega < 200\ s^{-1}$ or 30 Hz (at this frequency Fig. 7 shows that $\varepsilon_{SC} \approx 5000$ and $\rho_{SC} \approx 6 \times 10^4\ \Omega$ m).

The area of real (atomic) contact between two solids depends on the resolution of the instrument used to measure it and decreases with increasing resolution (*i.e.*, increasing magnification or decreasing pixel size). But, it also depends on the surface roughness so one cannot compare different cases directly without knowing the surface roughness (and the effective elastic modulus). For the human fingertip squeezed against a smooth counter-surface, many studies[35,36] have been presented where it appears that the contact area is ~50% of the nominal contact area. In our opinion, the area of atomic contact between dry skin and a flat counter surface is much smaller. Thus, neglecting the adhesion, the contact area may be of the order of $2p_0/(E^*h')$, where (typically) the squeezing pressure $p_0 \approx 10$ kPa, the effective modulus $E^* \approx 40$ MPa, and the rms slope (from surface topography measurements) $h' \approx 1$, giving $A/A_0 \approx 5 \times 10^{-4}$ or 0.05% relative contact. We attribute this difference between experimental observations and the theory to the limited resolution in experimental measurements and/or the existence of liquid in the contact region (sweat or oil), which makes the fluid filled interfacial region appear as real contact!

For example, Fig. 3 shows an optical picture of a glass surface where the oil–water fluid film left on the surface from a few seconds contact with the index finger. The fluid covers more than 50% of the apparent contact area. However, most of the friction between the finger and the glass surface is derived from the region of real skin–glass contact, or where the fluid film is very thin (in the order of a few nanometers or less).

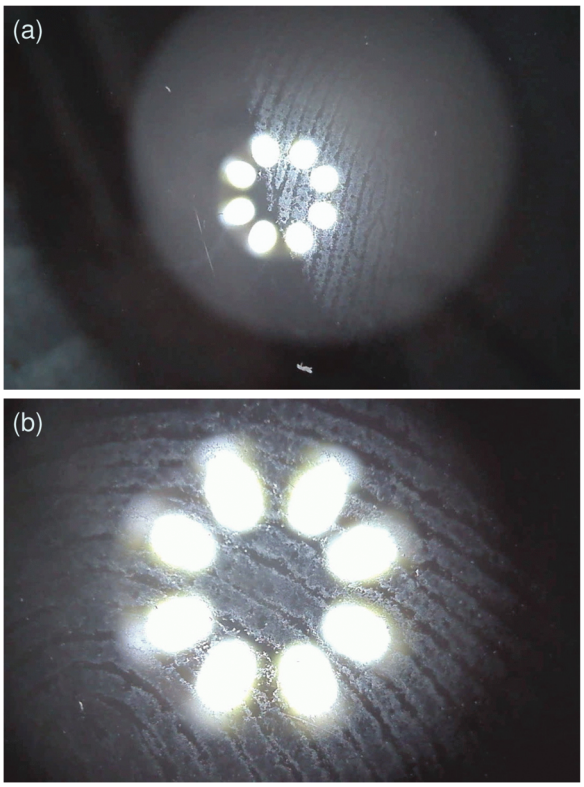

Fig. 3 Optical microscopy pictures at low (a) and high (b) magnifications of the fluid left on a glass surface after contact with the index finger. The fluid is mainly oil as it does not evaporate even after a long waiting time. If the finger is cleaned with soap and water, mainly water is deposited on the glass surface, which disappears a few seconds after removing the finger due to evaporation. The white elliptic regions are reflections in the glass surface of 8 light diodes.

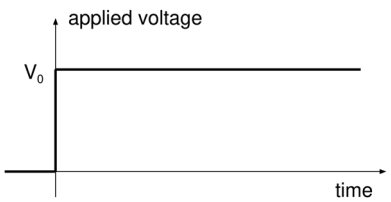

Fig. 4 A step-like change in the electric potential $\phi(t)$, where $\phi(t) = 0$ for $t < 0$ and $\phi(t) = V_0$ for $t > 0$.

2.2 Charge drift through the SC

We have argued above that if the frequency ω is small enough, the finite conductivity of the SC will result in transfer of mobile charges to the SC–air and SC–glass interfaces. Here we study this problem in more detail in the case where the electric potential $\phi(t)$ is turned-on in a step-like manner at time $t = 0$, see Fig. 4.

We define

$$\phi(\omega) = \frac{1}{2\pi}\int_{-\infty}^{\infty} dt\ \phi(t)e^{i\omega t}, \tag{14}$$

$$\phi(t) = \int_{-\infty}^{\infty} d\omega\ \phi(\omega)e^{-i\omega t}. \tag{15}$$

For the step function

$$\phi(\omega) = \frac{1}{2\pi}\int_0^{\infty} dt\ V_0 e^{-\varepsilon t}e^{i\omega t} = \frac{1}{2\pi i}\frac{V_0}{\omega + i\varepsilon}, \tag{16}$$

where we have included the factor $\exp(-\varepsilon t)$, with $\varepsilon = 0^+$ an infinitesimal positive number, in order to make the integral well defined. The electric field becomes

$$\begin{aligned} E_z &= \int_{-\infty}^{\infty} d\omega \frac{-\phi(\omega)}{u + h_0(\omega)}e^{-i\omega t}, \\ &= -\frac{1}{2\pi i}\int_{-\infty}^{\infty} d\omega\ V_0 \frac{1}{(u + h_0(\omega))(\omega + i\varepsilon)}e^{-i\omega t} \end{aligned} \tag{17}$$

Assuming that the dielectric function of the SC is of the form (13) with ε_{SC} and ρ_{SC} constants, we can write

$$\frac{1}{u+h_0(\omega)}=\frac{a\omega+ib}{\omega+i\gamma}, \tag{18}$$

where

$$\begin{aligned} a&=\frac{1}{u+d_1/\varepsilon_1+d_2/\varepsilon_{SC}},\\ b&=\frac{a}{\varepsilon_0\rho_{SC}\varepsilon_{SC}},\\ \gamma&=b(u+d_1/\varepsilon_1). \end{aligned} \tag{19}$$

We get

$$E_z=-\frac{V_0}{2\pi i}\int d\omega\frac{a\omega+ib}{\omega+i\gamma}\frac{1}{\omega+i\varepsilon}e^{-i\omega t} \tag{20}$$

We can calculate this integral by closing the integration path in the complex ω-space. This gives for $t > 0$:

$$E_z=V_0\left[\frac{b}{\gamma}+\left(a-\frac{b}{\gamma}\right)e^{-\gamma t}\right], \tag{21}$$

where

$$\frac{b}{\gamma}=\frac{1}{u+d_1/\varepsilon_1}. \tag{22}$$

For $t = 0$, we get from (21):

$$E_z=\frac{V_0}{u+d_1/\varepsilon_1+d_2/\varepsilon_{SC}}, \tag{23}$$

which corresponds to all the mobile charges located at the inner surface of the SC. For times $t \gg \tau$, where $\tau = 1/\gamma$, we have instead

$$E_z=\frac{V_0}{u+d_1/\varepsilon_1}, \tag{24}$$

which is the expected result when all the mobile charges are on the SC–air interface. Hence, the relaxation time

$$\tau=\varepsilon_0\rho_{SC}\varepsilon_{SC}\left(1+\frac{d_2/\varepsilon_{SC}}{u+d_1/\varepsilon_1}\right), \tag{25}$$

describes the time it takes for the mobile charges to move from the inner surface of the SC to the outer surface at the air interface. In reality, the glass substrate may have a finite electric surface conductivity, and a fraction of the mobile charges may leave the SC and distribute themselves on the glass surface. This would result in a reduction of the electric attraction between the finger and the skin.

One interesting experiment would be to measure the friction force as a function of time after applying the voltage at time $t = 0$. This would contain information about the charge transfer from the inner to the outer surface of the SC and maybe even to the glass surface. We also note that if there is a fluid with ions, *e.g.*, sweat due to the finger (moisture), in the nominal contact region, the electric potential in the gap between the finger and the countersurface is influenced.

3 Materials and methods

3.1 Skin model

Human skin is a very complex material with non-homogeneous and non-linear viscoelastic properties. Here, we will use a simplified description which we believe is sufficient for modeling contact interactions with a touchscreen under electroadhesion.

3.1.1 Surface roughness. The surface topography of (dry and wet) human wrist skin was already investigated by using optical and atomic force microscopy.[30,31] From the measured topography, the surface roughness power spectrum was obtained. The red curve in Fig. 5 shows the surface roughness power spectrum of undeformed dry wrist skin as a function of the wavenumber (log–log scale). The surface has an rms roughness amplitude of 22 μm and an rms slope of 0.91. The linear region for $q > 4 \times 10^5$ m^{-1} corresponds to a Hurst exponent $H = 0.86$. Using the roughness power spectrum of wrist skin as a reference, power spectrum curves for finger skin are constructed for different values of E_{SC}. The green and blue curves are the power spectra of plastically deformed finger skin surfaces (obtained as described in Appendix A) assuming that the Young's modulus of the stratum corneum is E_{SC} = 100 MPa and E_{SC} = 1 GPa, respectively, and the penetration hardness is σ_Y = 50 MPa. For E_{SC} = 10 MPa and E_{SC} = 1 MPa, no plastic deformation occurs, and in those cases we have used the power spectrum given by the red curve in Fig. 5. Some calculations given below are performed with either a 4 times higher or 4 times smaller power spectrum in magnitude. These surfaces have rms roughness amplitudes of 44 μm and 11 μm, respectively.

3.1.2 Mechanical properties. We treat the skin using a two layer model shown in Fig. 6. The bulk has a Young's elastic modulus denoted by E_{bulk} and a Poisson ratio ν_{bulk} of 0.5.

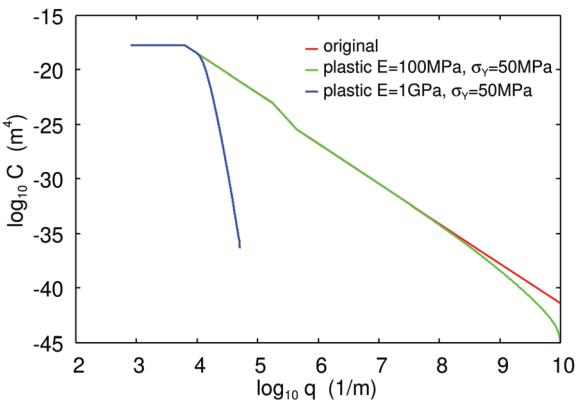

Fig. 5 The surface roughness power spectrum as a function of the wavenumber (log–log scale). The power spectrum of the undeformed surface (red line) has an rms roughness amplitude of 22 μm and an rms slope of 0.91. The linear region for $q > 4 \times 10^5$ m^{-1} corresponds to a Hurst exponent $H = 0.86$. The green and blue lines are the power spectra of the plastically deformed surfaces assuming E_{SC} = 100 MPa and E_{SC} = 1 GPa, respectively, and a penetration hardness of 50 MPa. For the plastic deformation calculations, we assume that the thickness of the SC is 200 μm and the elastic modulus of the tissue under the SC is E_{bulk} = 10 kPa. The plastically smoothed surface profiles have rms roughnesses of 22 μm (green curve) and 20 μm (blue curve).

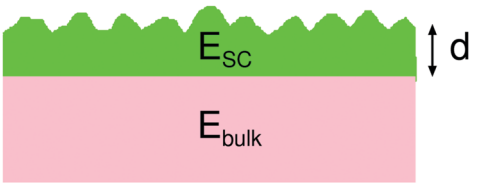

Fig. 6 The model of the skin used in the theoretical calculations. The bulk elastic modulus is E_{bulk} = 10–30 kPa and the Poisson ratio is ν_{bulk} = 0.5. The top layer (stratum corneum) is d = 100–200 μm thick and has a Young's modulus of $E_{SC} \approx$ 1–10 MPa in the wet state and $E_{SC} \approx$ 0.1–1 GPa in the dry state and the Poisson ratio is ν_{SC} = 0.5.

The top layer [stratum corneum (SC)] has the thickness d_2, the Young's modulus E_{SC} and the Poisson ratio ν_{SC} = 0.5. Since the thickness of the top layer and its elastic modulus can vary largely from one individual to another,[37] we have considered a range of parameters in our modeling calculations, namely

(a) E_{SC} = 1, 10, 100, 1000 MPa
(b) d_2 = 100, 200, 300, 400 μm
(c) E_{bulk} = 3, 10, 30 kPa

The large variation in E_{SC} is considered in this study to reflect the strong dependency of the elastic modulus of the SC on the humidity: E_{SC} decreases from ≈1 GPa in the dry state to 10 MPa (or less) in the wet state.[38–41] In the dry state, when the skin is squeezed against a hard counter surface, the contact pressure becomes so high that plastic deformation of the SC occurs in the asperity contact regions. In the study below, we take this into account by setting the penetration hardness to σ_Y = 50 MPa.[30,31,42] We note that the plastic deformation of the SC is unlikely to involve breaking of strong covalent bonds, but rather involves moving segments of polymers over energetic barriers, which are too high to be rapidly overcome by thermal fluctuations in the dry state. However, if the plastically deformed SC is exposed to high enough humidity, it swells, and the energetic barriers for segmental motion are reduced. In that case, the thermal motion can rearrange the polymer chains so that the SC takes its original undeformed state on return to the dry state. This situation is very similar to the behavior of rubber when plastically deformed at low temperatures.[43] The elastoplastic linear model we use for the SC is relatively simple. A better, but more complex description would be a nonlinear viscoelastic model.

3.1.3 Electrical properties. The dielectric properties of human skin have been measured by Yamamoto *et al.*[34] In Fig. 7, we show the variation in dielectric constant and the electrical resistivity as a function of the stimulation frequency. In the frequency range of interest, from f = 0 (static) to f = 1000 Hz, ε_{SC} decreases from ≈10^4 to ≈10^3. The dielectric function (and electrical conductivity) of the bulk tissue under the SC is higher than that of the SC and will be considered as perfectly conducting in our analysis.

3.2 Touchscreen related parameters

In our model, the insulator thickness d_1 and dielectric constant ε_1 of the touchscreen (the rigid solid with a flat surface shown in Fig. 1) were determined for the capacitive touchscreen

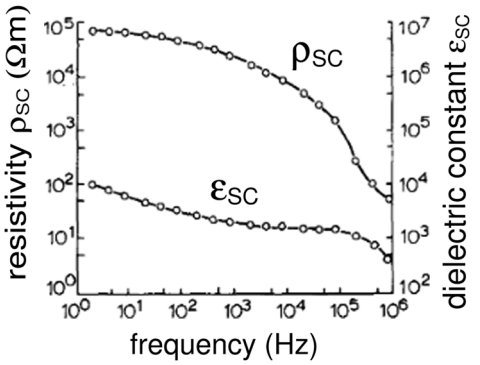

Fig. 7 The dielectric constant and the resistivity of the human SC as a function of the simulation frequency (adopted from Yamamoto *et al.*[34]).

(Model: SCT-3250, 3M) used in our experiments (see Section 4). A field emission scanning electron microscopy (FESEM, Zeiss Ultra Plus) analysis was performed on the touchscreen to measure the thickness of the insulating layer. Fig. 8 presents cross-sectional FESEM images of the touchscreen. The image on the left is acquired by the secondary electron detector and displays the topography. The image on the right is simultaneously collected with the in-lens detector and emphasizes the material contrast. The conductive layer appears with bright contrast, whereas the top insulator layer appears in black. The image also shows that the top insulator has a different composition from the substrate glass. The sample was imaged without a conductive carbon or gold coating. We identified 3 main layers through the measurement: an electrical insulator layer (SiO_2) with a thickness of $d_1 \approx$ 1 μm, an electrical conducting layer (ITO) with a thickness of ≈250 nm, and a glass substrate. The dielectric constant of the insulator layer $\varepsilon_1 \approx$ 3.9–10 is used below.[44–46] The effective thickness of the insulating layer $h_0 = d_1/\varepsilon_1 + d_2/\varepsilon_2$ is not exactly known since the thickness d_2 and the dielectric constant ε_{SC} of the SC are highly dependent on the subject.[47]

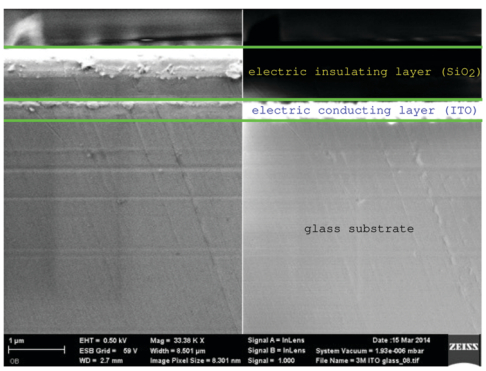

Fig. 8 Cross-sectional images of the capacitive touchscreen (Model: SCT-3250, 3M) obtained by field emission scanning electron microscopy (FESEM, Zeiss Ultra Plus). The image on the left shows the layers of the touchscreen. The image on the right is collected simultaneously by its in-lens detector to obtain a better contrast for differentiating the layers. There are three main layers: an electrical insulator layer (SiO_2) with a thickness of ≈1 μm, an electrical conducting layer (ITO) with a thickness of ≈250 nm, and a glass substrate.

3.3 Sliding friction experiments on a touchscreen with a human finger

The effect of the voltage applied to the conductive layer of the touchscreen on the friction force F_f was investigated as a function of the normal force applied to the touchscreen by the sliding index finger, and the results were compared with those obtained from theory.

The major components of our set-up include a high-torque step motor moving a slider on a power screw and a force sensor attached to the base of the touchscreen (Model: SCT-3250, 3M) and are shown in Fig. 9. The step motor (MDrive23Plus, Intelligent Motion Systems Inc.) was programmed to translate the slider forward and backward in the horizontal direction at the desired sliding velocity. The experimenter's hand was placed on the slider such that the phalanges of the index finger were aligned with a constant angle of approximately 30° with respect to the touchscreen, and the tip of the index finger was always in contact with the touchscreen during the sliding. A sinusoidal voltage signal with each of the following amplitudes 25 V, 50 V, 75 V, 100 V, 125 V, 150 V, 175 V, and 200 V at 125 Hz was applied to the touchscreen. As the experimenter's finger was moving on the touchscreen, the force response was measured using a force transducer (Nano17, ATI Industrial Automation Inc.) placed under the touchscreen. The normal and tangential forces were acquired using a 16-bit analog data acquisition card (NI PCI-6034E, National Instruments Inc.) with a sampling rate of 10 kHz. Note that the electric stress oscillates between zero and a value twice as large as the average electric stress, although the voltage applied to the touchscreen takes negative and positive values, and oscillates around zero. If we assume that the friction force F_f is proportional to the sum of the applied stress p_0 and the adhesive stress (3), then we expect the friction force to oscillate with the frequency $2\omega_0$, where ω_0 is the frequency of the voltage signal applied to the touchscreen.

To illustrate that this is indeed the case, in Fig. 10 we show the measured friction force F_f as a function of time. The green-colored data are with the applied oscillating electric potential

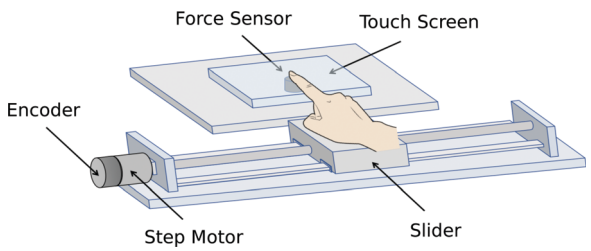

Fig. 9 The experimental setup used to measure the force response of the index finger in the normal and tangential directions *via* a force transducer (Nano17, ATI Industrial Automation Inc.) placed under the touchscreen (Model: SCT-3250, 3M) as a function of applied voltage V. The experimenter's hand was placed on the slider driven by a step motor (MDrive23Plus, Intelligent Motion Systems Inc.) such that the phalanges of the index finger were aligned with an angle of approximately 30° with respect to the touchscreen, and the tip of the index finger was always in contact with the touchscreen during the forward and backward translation of the slider along the horizontal direction.

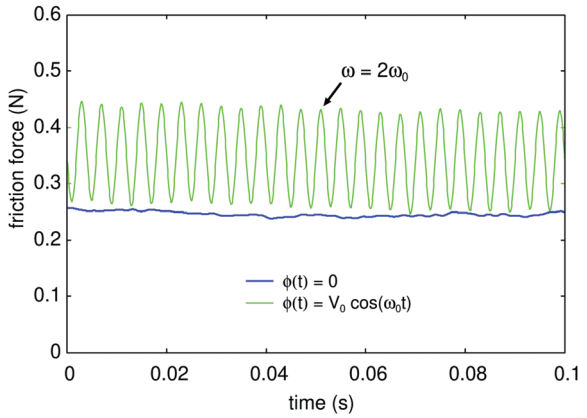

Fig. 10 The friction force F_f as a function of time. Green-colored data: with an applied oscillating electric potential $\phi(t) = V_0\cos(\omega_0 t)$ (V_0 = 100 V and $f_0 = \omega_0/(2\pi)$ = 125 Hz). Blue-colored data: without an applied electric potential. The normal force is F_N = 1 N in both cases. Note that there are 25 oscillations in the green-colored data, *i.e.*, the frequency of oscillations in the electric stress is 25/0.1 = 250 Hz, *i.e.*, twice the frequency of the applied electric potential.

$\phi(t) = V_0\cos(\omega_0 t)$ (V_0 = 100 V and $\omega_0 = 2\pi f_0$ with f_0 = 125 Hz), while the blue-colored data are the friction force without an applied electric potential. The blue-colored data are slightly below the green data because the applied normal force was slightly lower in the case of no applied voltage.

The finger of the experimenter moved forward and backward on the touchscreen for a total displacement of 80 mm in one cycle. The sliding velocity was selected as 50 mm s^{-1} based on the preliminary experiments such that full slip behavior was observed between the fingertip and the touchscreen. For each applied voltage, the experimenter aimed to increase his normal force from 0.2 N to 2 N with an increment of 0.2 N after every other 4 cycles. In order to keep the normal force constant, the test person visually tracked his force response from a large screen oscilloscope and trained himself in advance of the experiments. However, it is important to emphasize that keeping the normal force at a constant value was not easy even for a trained experimenter and some deviations occurred. The electrovibration was turned on and off after every other cycle. Hence, the experimenter made a total number of 320 cycles (8 different applied voltages × 10 increments of normal force per applied voltage × 2 cycles per force increment × 2 experimental conditions (*i.e.*, electrovibration on *versus* off)).

All the experiments were carried out at room temperature (22 °C). The fingerpad of the subject and the glass of the touchscreen were cleaned with ethanol before each measurement. An external fan, placed near the sliding mechanism, was used to hinder the accumulation of moisture on the fingerpad.

4 Theory: numerical results

Let us now present some numerical results. We assume that the skin is in contact with a touchscreen. The touchscreen is assumed to consist of a conducting layer covered with a thin insulating layer (thickness d_1) as in Fig. 1. In the theory section,

we have defined the effective thickness of the insulating layers as $h_0 = d_1/\varepsilon_1 + d_2/\varepsilon_2$. Assuming $d_1 = 1$ μm and that the insulating layer is made of silicone dioxide so that $\varepsilon_1 \approx 3.9$, we get $d_1/\varepsilon_1 \approx 0.26$ μm. If we assume that the SC has a thickness d_2 of ≈200 μm and a dielectric constant ε_2 of ≈3000 (see Fig. 7), we get $d_2/\varepsilon_2 \approx 0.07$ μm.[47,48] For the frequency $f = 0$ (static), $\varepsilon_2 \approx 10^4$, giving $d_2/\varepsilon_2 \approx 0.02$ μm. Thus, it appears that the insulating film on the substrate will give the largest contribution to h_0, and that it should be possible to reduce h_0 to ≈0.1 μm by reducing the thickness of the insulating film. In the following, unless otherwise stated, we will assume $h_0 = 0.3$ μm but we also show some results for $h_0 = 0.1$ μm and $h_0 = 1$ μm. Hence, our reference system has the nominal values of $h_0 = 0.3$ μm, $d_2 = 200$ μm, $E_{\text{bulk}} = 10$ kPa, $E_{\text{SC}} = 100$ MPa, and the power spectrum given by the green curve in Fig. 5 (which takes into account the plastic deformation). The applied squeezing pressure is $p_0 = 10$ kPa, so finite size effects are unimportant (see Appendix A). In each of the following subsections, we investigate the influence of one parameter while fixing the others.

4.1 Power spectrum $C(q)$

Fig. 11 shows the normalized contact area A/A_0, and the average surface separation $\bar{u}$ as a function of the applied voltage V for the surface roughness power spectrum shown in Fig. 5 (green curve), and those with 4 times higher and 4 times lower power spectrum (solid and dashed red curves). The thickness of the effective insulating layer is $h_0 = d_1/\varepsilon_1 + d_2/\varepsilon_2 = 0.3$ μm. The results show an increase in the normalized contact area A/A_0, when the power spectrum of the plastically deformed surface (solid red) is used, compared to that without plastic deformation (dashed red). On the other hand, the normalized contact area A/A_0 is decreased when the surface rms-roughness is increased. The average separation between the surfaces has a negative correlation with the normalized contact area A/A_0. As expected, the average separation between the surfaces is reduced as the rms roughness amplitude is lowered.

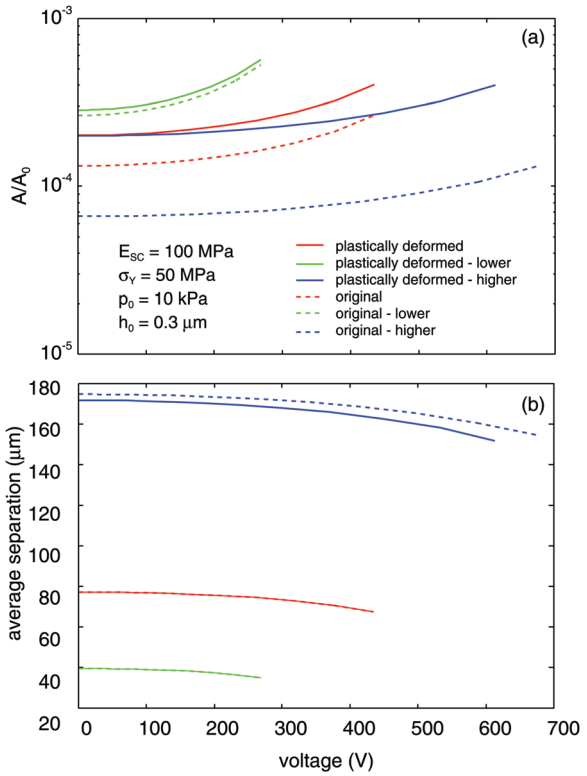

Fig. 11 The normalized contact area A/A_0 (a), and the average surface separation $\bar{u}$ (b), as a function of the applied voltage V. We have used the surface roughness power spectrum shown in Fig. 5 (rms roughness = 22 μm), and those with 4 times higher and 4 times lower surface roughnesses (rms roughnesses = 44 μm and 11 μm, respectively). We assumed the Young's modulus of the SC as $E_{\text{SC}} = 100$ MPa without plasticity (dashed curves) and with plasticity considering a penetration hardness of $\sigma_Y = 50$ MPa (solid curves). The thickness of the effective insulating layer is $h_0 = d_1/\varepsilon_1 + d_2/\varepsilon_2 = 0.3$ μm. The Young's modulus of the bulk material is $E_{\text{bulk}} = 10$ kPa. The applied pressure is $p_0 = 10$ kPa. Note that the curves of average separation for the plastically deformed (solid red) and original (dashed red), and also plastically deformed – lower (solid green) and original – lower (dashed green) surfaces overlap (bottom figure).

4.2 Young's modulus E_{SC} of the SC

Fig. 12 shows the normalized contact area A/A_0 (a), and the average surface separation $\bar{u}$ (b), as a function of the applied voltage V. The thickness of the effective insulating layer is $h_0 = d_1/\varepsilon_1 + d_2/\varepsilon_2 = 0.3$ μm, the Young's modulus of the bulk material is $E_{\text{bulk}} = 10$ kPa, and the applied pressure is $p_0 = 10$ kPa. The results demonstrate that when the Young's modulus of the SC increases, the normalized contact area A/A_0 decreases, while the average surface separation $\bar{u}$ increases. Enabling plasticity for $E_{\text{SC}} = 1$ GPa results in an increase in the normalized contact area and a decrease in the average surface separation.

4.3 Thickness d_2 of the SC

In order to evaluate the effect of the SC thickness on the normalized contact area A/A_0, and the average surface separation $\bar{u}$ as a function of the applied voltage V, simulations are performed using the thickness values reported in the literature.[48] The Young's modulus of the SC is taken as $E_{\text{SC}} = 100$ MPa with the power spectrum shown by the green curve in Fig. 5, the applied pressure is $p_0 = 10$ kPa, and the thickness of the effective insulating layer is $h_0 = d_1/\varepsilon_1 + d_2/\varepsilon_2 = 0.3$ μm. Fig. 13 shows that when the thickness of the SC decreases, the normalized contact area A/A_0 increases, while the average surface separation decreases.

4.4 Effective thickness h_0 of the insulating layer

Fig. 14 shows the influence of the thickness of the effective insulating layer h_0 on the normalized contact area A/A_0, and the average surface separation $\bar{u}$ as a function of the applied voltage V. The thickness of the effective insulating layer is varied based on the possible variations in the parameters of $h_0 = d_1/\varepsilon_1 + d_2/\varepsilon_2$. The Young's modulus of the SC is taken $E_{\text{SC}} = 100$ MPa with the power spectrum shown by the green curve in Fig. 5, and the applied pressure is $p_0 = 10$ kPa. The results show that the thickness of the effective insulating layer has a significant impact on the normalized contact area and the average surface separation for the values varying between $h_0 = 0.1$ and 0.4 μm. As h_0 is decreased, the normalized contact area is enlarged, while the average surface separation is reduced.

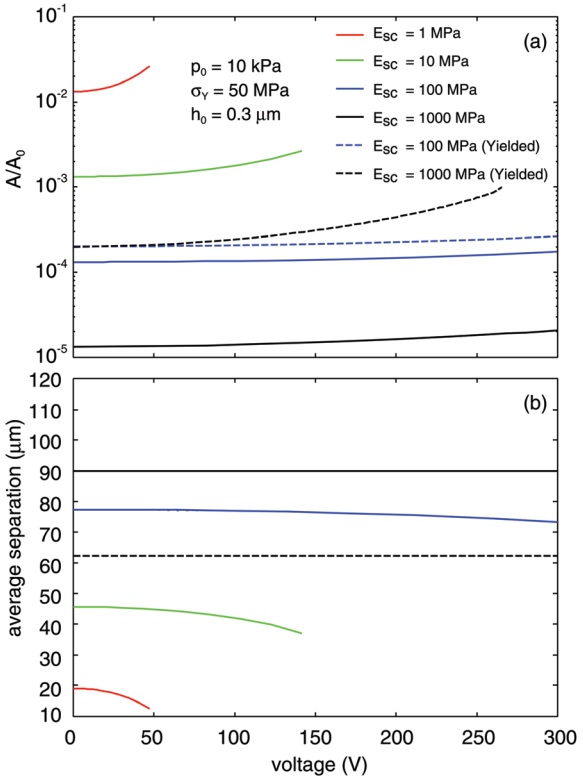

Fig. 12 The normalized contact area A/A_0 (a), and the average surface separation $\bar{u}$ (b), as a function of the applied voltage V. The Young's moduli of the SC are taken as E_{SC} = 1 MPa (red), E_{SC} = 10 MPa (green), E_{SC} = 100 MPa (blue), E_{SC} = 1000 MPa (black), E_{SC} = 100 MPa with plasticity, assuming a penetration hardness of σ_Y = 50 MPa (dashed blue), and E_{SC} = 1000 MPa with plasticity, assuming a penetration hardness of σ_Y = 50 MPa (dashed black). The thickness of the effective insulating layer is $h_0 = d_1/\varepsilon_1 + d_2/\varepsilon_2$ = 0.3 μm. The Young's modulus of the bulk material is E_{bulk} = 10 kPa. The applied pressure is p_0 = 10 kPa. Note that the curves for E_{SC} = 100 MPa (blue) and E_{SC} = 100 MPa (yielded, dashed blue) overlap on top of each other at the bottom figure.

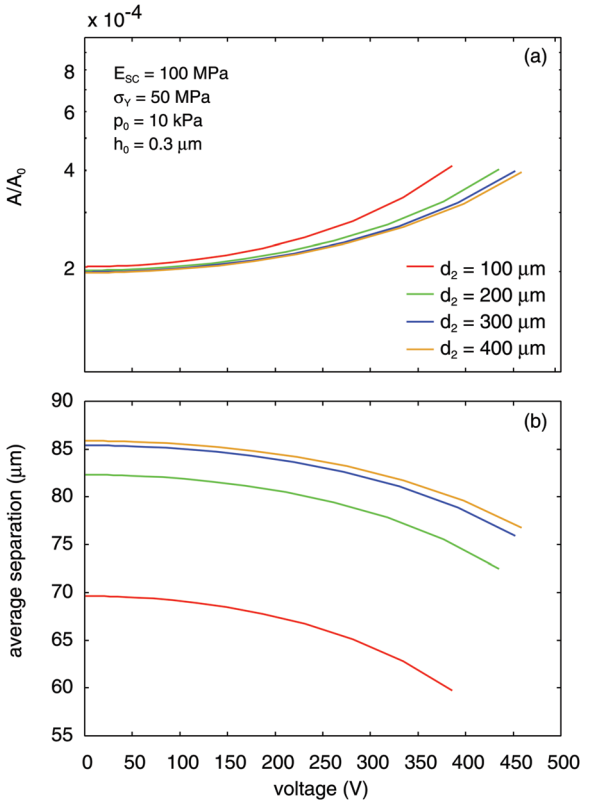

Fig. 13 The normalized contact area A/A_0 (a), and the average surface separation $\bar{u}$ (b), as a function of the applied voltage V. The thickness of the SC is d_2 = 100 μm (red), d_2 = 200 μm (green), d_2= 300 μm (blue), and d_2= 400 μm (yellow). The Young's modulus of the SC is E_{SC} = 100 MPa, the penetration hardness is σ_Y = 50 MPa, the power spectrum is the green curve in Fig. 5, and the Young's modulus of the bulk material is E_{bulk} = 10 kPa.

4.5 Applied nominal contact pressure p_0

The influence of the applied contact pressure p_0 on the normalized contact area A/A_0, and the average surface separation $\bar{u}$ are shown in Fig. 15. The contact pressure is selected in the range of p_0 = 1–100 kPa based on the typical pressures applied by the finger to the touchscreen. As expected, the results show that the normalized contact area increases with the applied contact pressure, while the average surface separation decreases.

4.6 Probability distribution of electro-adhesive stress

The contact between randomly rough surfaces results in physical quantities which fluctuate strongly depending on the location at the interface. In addition, some properties may differ for each realization of the system. In this case it is useful to consider the probability distribution of a property. The probability distributions for the interfacial separation, the electric field strength in the gap, and the interfacial stress acting on the solid walls, have been presented in ref. 49. Here we consider the probability distribution of the attractive electric stress.

Let $P_u(u)$ and $P_\sigma(\sigma)$ be the probability distributions for the separation u and the attractive electric stress σ acting on the outer surface of the skin from the touchscreen. The probability distributions are assumed to be normalized so that, *e.g.*,

$$\int_0^\infty \mathrm{d}u\ P_u(u) = \int_0^\infty \mathrm{d}\sigma\ P_\sigma(\sigma) = 1$$

Let us derive the distribution of attractive stress due to the electric field in the air gap. The electric stress

$$\sigma = \frac{1}{4}\frac{\varepsilon_0 V_0^2}{(u+h_0)^2}. \tag{26}$$

Thus we get

$$\mathrm{d}\sigma = -\frac{1}{2}\frac{\varepsilon_0 V_0^2}{(u+h_0)^3}\mathrm{d}u.$$

From

$$\int_0^\infty \mathrm{d}u\ P_u(u) = \int_0^\infty \mathrm{d}\sigma\ P_\sigma(\sigma) = \int_0^\infty \mathrm{d}u\ P_\sigma \frac{1}{2}\frac{\varepsilon_0 V_0^2}{(u+h_0)^3}$$

we get

$$P_\sigma = \frac{2(u+h_0)^3}{\varepsilon_0 V_0^2} P_u \tag{27}$$

Using (26) and (27) it is easy to plot P_σ as a function of σ given P_u as a function of u.

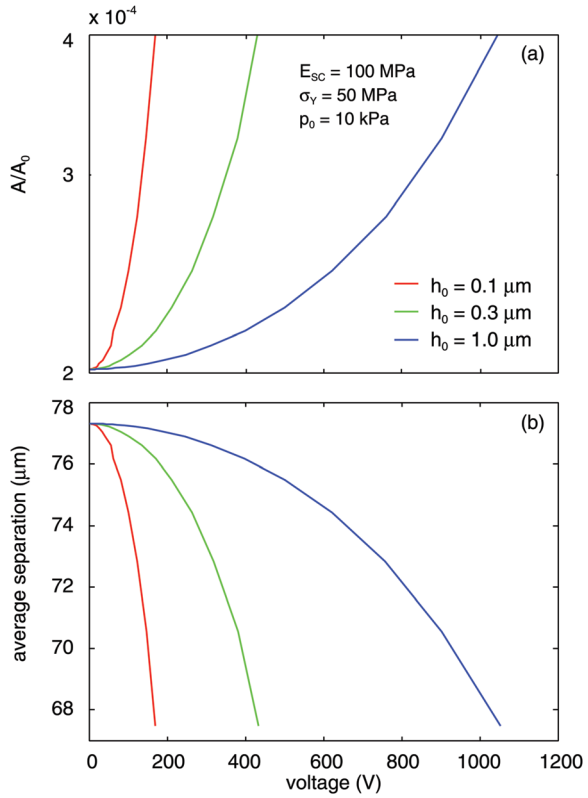

Fig. 14 The normalized contact area A/A_0 (a), and the average surface separation $\bar{u}$ (b), as a function of the applied voltage V. The thickness of the effective insulating layer is taken as $h_0 = d_1/\varepsilon_1 + d_2/\varepsilon_2 = 0.1$ μm (red), 0.3 μm (green) and 1 μm (blue). The Young's modulus of the SC is $E_{SC} = 100$ MPa with plasticity (penetration hardness $\sigma_Y = 50$ MPa), assuming the power spectrum shown by the green curve in Fig. 5. The Young's modulus of the bulk material is $E_{bulk} = 10$ kPa, and the applied pressure is $p_0 = 10$ kPa.

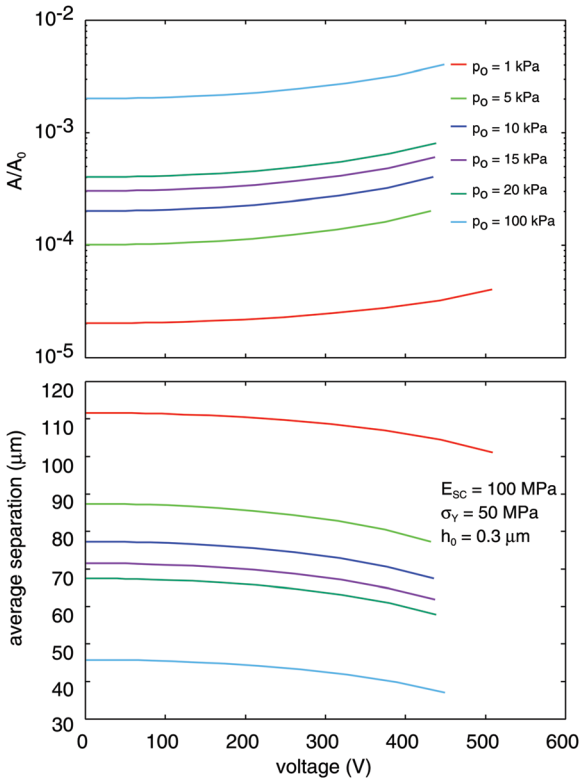

Fig. 15 The normalized contact area A/A_0 (a), and the average surface separation $\bar{u}$ (b), as a function of the applied voltage V. The applied squeezing pressure p_0 is varied in the range of p_0 = 1–100 kPa. The thickness of the effective insulating layer is $h_0 = d_1/\varepsilon_1 + d_2/\varepsilon_2 = 0.3$ μm. The SC Young's modulus is $E_{SC} = 100$ MPa with plasticity (penetration hardness $\sigma_Y = 50$ MPa), assuming the power spectrum shown by the green curve in Fig. 5. The Young's modulus of the bulk material is $E_{bulk} = 10$ kPa.

Fig. 16(a) shows the probability distribution of the adhesive electric stress acting on the outer skin surface in the nominal skin–glass contact area. In most of the skin area the adhesive stress is very small, of the order of 1–100 Pa, but this surface area gives a negligible contribution to the total attractive electrostatic force. This can be shown as follows:

To understand which region in space gives the biggest contribution to the electric adhesion force, we consider the average adhesive stress

$$\langle\sigma\rangle = \int_0^\infty \mathrm{d}\sigma\ \sigma P_\sigma(\sigma)$$

Let us introduce a new integration variable $x = \log_{10}(\sigma)$ so that $\mathrm{d}\sigma = \ln(10)\sigma\mathrm{d}x$ and

$$\langle\sigma\rangle = \int_{-\infty}^\infty \mathrm{d}x\ S(x),$$

where

$$S = \ln(10)\sigma^2 P_\sigma(\sigma).$$

Thus $S(x)\mathrm{d}x$ is the contribution to the average stress from the region where the logarithm of the stress is between $x = \log_{10}\sigma$ and $x + \mathrm{d}x = \log_{10}\sigma + \mathrm{d}\log_{10}\sigma$. In Fig. 16(b) we show $\log_{10}S$ as a function of $x = \log_{10}\sigma$. Clearly the most important contribution to the adhesive normal load comes from the region where the stress is close to the maximum stress $\sigma_{max} = \varepsilon_0 V_0^2/(4h_0^2)$ indicated by the vertical dashed line. This region in σ-space corresponds to the area of real contact and the region close to the area of real contact, where the skin–touchscreen surface separation is very small; this region is denoted as the rim-area.

5 Comparison of the theory with the experiment

The friction force F_f and the normal force F_N (markers) measured as a function of the applied voltage V are presented in Fig. 17. The voltage applied to the conductive layer of the touchscreen varies from 0 V to 200 V with an increment of 25 V at 125 Hz. The results show that the friction force increases with normal force for the range of F_N = 0.2–2 N. Also, the friction force increases when the applied voltage is increased. Note that the relative increase in the friction force with voltage is in good agreement with the theory, suggesting that the electrostatic force is proportional to the square of the applied voltage.

We also measured the apparent contact area of the fingertip of the experimenter at different normal loads from the high-contrast

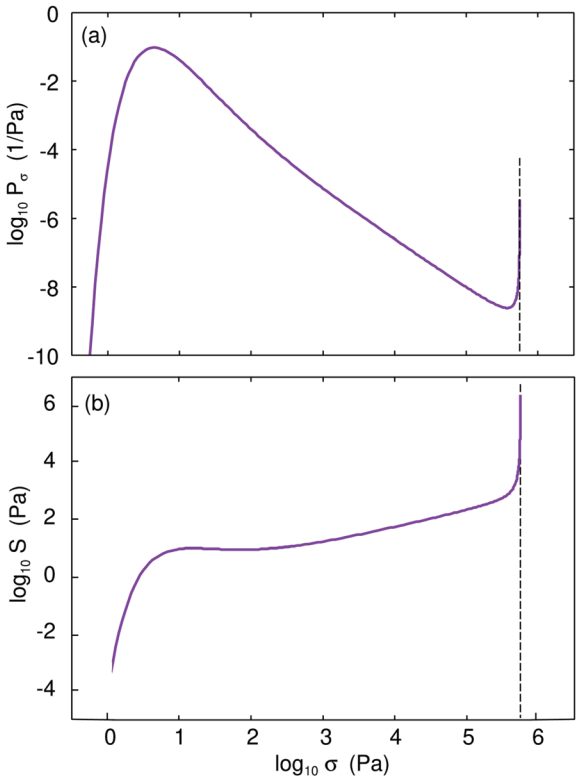

Fig. 16 (a) The probability distribution $P_\sigma(\sigma)$ of the electric attraction stress. The logarithm of $P_\sigma(\sigma)$ is shown as a function of the logarithm of the electric stress. (b) The logarithm of the function S as a function of the logarithm of the electric stress (see text for details). The vertical dashed line indicates the maximum electric stress $\sigma = \varepsilon_0 V_0^2/(4h_0^2)$ (for E_{SC} = 40 MPa, h_0 = 0.2 μm, and the applied voltage amplitude V_0 = 100 V).

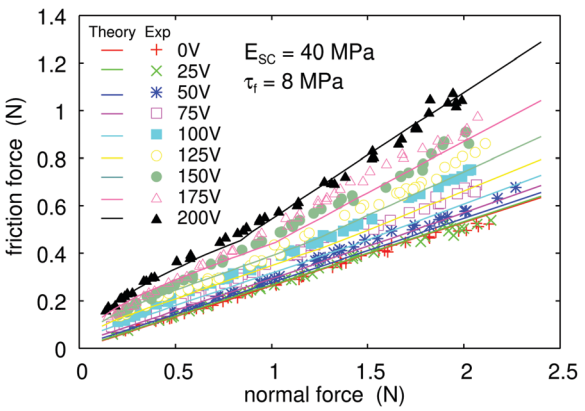

Fig. 17 The friction force F_f obtained from the theory (solid curves) and the experiments (markers) as a function of the applied normal force F_N. The voltage applied to the conductive layer of the touchscreen is varied from 0 V to 200 V with an increment of 25 V at 125 Hz. The speed of the sliding finger during the experiments was 50 mm s^{-1}. In the model, we set E_{SC} = 40 MPa, d = 200 μm, E_{bulk} = 10 kPa and h_0 = 0.2 μm. The shear stress is assumed to be τ_f = 8 MPa, which is consistent with τ_f = 5 MPa for wet skin and τ_f = 13 MPa for dry skin.[30,31]

fingerprint images obtained using a coaxial light source and camera. The apparent contact area A_0 depends weakly on the normal force $A_0 \sim F_N^{0.1}$. Since we argue that the real contact area is more important than the nominal contact area for the contact mechanics and friction, we will not discuss the results any further here.

In the relevant range of nominal contact pressures, the theory predicts that the relative contact area A/A_0 is nearly proportional to the applied nominal contact pressure p_0. Assume that the frictional shear stress τ_f acting on the area of real contact is independent of p_0, as expected from the theory when the local pressure in the asperity contact regions is small enough, or when the pressure in the contact regions is nearly constant. In this case, it follows that the friction force $F_f = \tau_f A = \tau_f(A/A_0)A_0$ is nearly proportional to the normal force $F_N = A_0 p_0$, and we can obtain the relationship between F_f and F_N directly from the relationship between A/A_0 and p_0.

In Fig. 17 we compare the friction force F_f measured as a function of the normal force with the one predicted by the theory (solid curves). The frictional shear stress τ_f was adjusted to obtain the best possible fit with respect to the measured data, and the value used for that, τ_f = 8 MPa, is consistent with τ_f = 5 MPa for wet skin and τ_f = 13 MPa for dry skin.[30,31]

Note that when the electroadhesion is on, the measured friction force extrapolates to a finite value as the applied normal force extrapolates to zero. In the present case, this is due to the finite-size effect: a finite system has asperities of finite height, and the average surface separation is finite even as the normal force approaches zero. Hence, when the electroadhesion is on, there will always be an attractive force acting between the solids and a finite area of real contact, which results in non-zero friction force during sliding.

In Fig. 18 we show the friction coefficient obtained from the theory (solid curves) and the experiments (markers) as a function of the applied normal force F_N. The voltage applied to the conductive layer of the touchscreen is varied from 0 V (red) to 200 V (black). The figure is based on the experimental and theoretical data presented in Fig. 17. Note that the friction coefficient increases when the applied normal force decreases.[50] This is a typical behavior when adhesion is important. Note that a

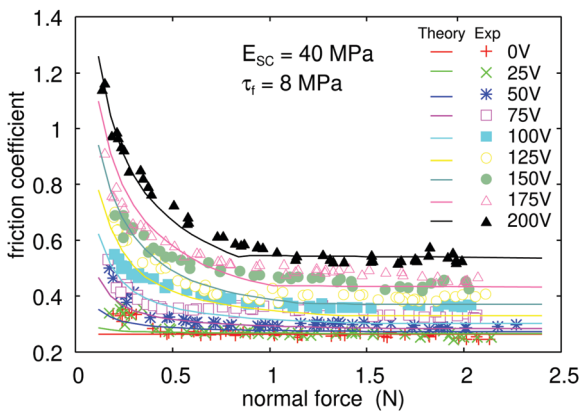

Fig. 18 The friction coefficient μ obtained from the theory (solid curves) and the experiments (markers) as a function of the applied normal force F_N. The voltage applied to the conductive layer of the touchscreen is varied from 0 V (red) to 200 V (black). Based on the experimental and theoretical data presented in Fig. 17.

small increase in the friction coefficient is also obtained when the applied voltage is turned off. This has been observed also in earlier studies,[38] and must be due to some additional adhesion process, *e.g.*, due to the van der Waals interaction, or due to capillary bridges formed by moisture or oil on the finger.[21] Since electroadhesion is the only attractive interaction included in the theory, the increase in friction coefficient as the applied normal force approaches zero for $V = 0$ cannot be described by the proposed theory yet.

Fig. 19 shows the calculated dependency of the contact area on the frequency $f = \omega/(2\pi)$ of the oscillating electric potential $\phi = V_0\cos(\omega t)$. The A_{on}/A_{off} ratio of the real contact area with electroadhesion to that without electroadhesion was obtained using (10) with the dielectric function $\varepsilon_2(\omega)$ of the SC given by (13) with $\varepsilon_{SC}(\omega)$ and $\rho_{SC}(\omega)$ given in Fig. 7. We have used the normal force $F_N = 0.5$ N, $V_0 = 100$ V, $d_1 = 1$ μm, and $d_2 = 200$ μm. Fig. 19(a) shows A_{on}/A_{off} for three different touchscreen glass dielectric constants, $\varepsilon_1 = 4$, 8 and 10.

At low frequencies the charge on the skin surface can drift out on the touchscreen. This effect depends on the surface and bulk electrical conductivities of the touchscreen, and on liquids (*e.g.* oil and sweat) which may occur in some fraction of the non-contact area. To take this into account, we also show calculated results in Fig. 19(b), where we assume that the airgap is filled with materials with resistivities ρ equal to 10^5, 10^6 and 10^7 Ω m.

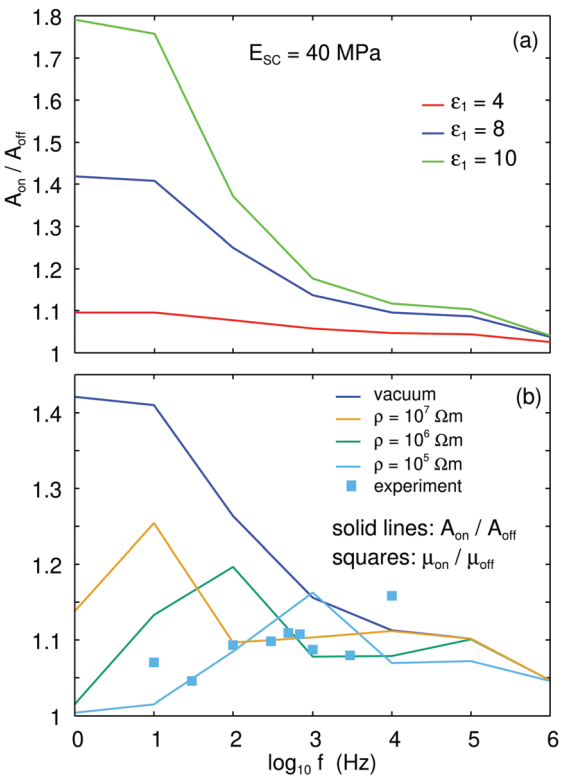

Fig. 19 The calculated dependency of the contact area on the frequency $f = \omega/(2\pi)$ of the oscillating electric potential $\phi = V_0\cos(\omega t)$. The A_{on}/A_{off} is the ratio of the real contact area with electroadhesion to that without electroadhesion, obtained using (10) with the dielectric function $\varepsilon_2(\omega)$ of the SC given by (13) with $\varepsilon_{SC}(\omega)$ and $\rho_{SC}(\omega)$ given in Fig. 7. We have used the normal force $F_N = 0.5$ N, $V_0 = 100$ V, $d_1 = 1$ μm, and $d_2 = 200$ μm. In (a) we show results for $\varepsilon_1 = 4$, 8 and 10 assuming a vacuum (or air) gap, while in (b) $\varepsilon_1 = 8$ and the gap between the solids has a nonzero electrical conductivity so that the charge on the skin surface can drift out on the touchscreen.

If we assume that the friction force is proportional to the area of real contact, then the A_{on}/A_{off} ratio equals the μ_{on}/μ_{off} ratio of the friction coefficient with electroadhesion to that without electroadhesion. The square symbols in Fig. 19(b) are experimental data for the μ_{on}/μ_{off} ratio. Similar results were obtained by Meyer *et al.*[1] (see also ref. 51 for measurements using current controlled induction).

Note that as the frequency ω decreases, the mobile charges on the skin will move from the inner interface between the SC and the tissue below to the outer SC–air (or SC–glass) interface. In Section 2.2, we showed that this occurs on the time scale of $\tau \approx \varepsilon_0\rho_{SC}\varepsilon_{SC} \approx 3 \times 10^{-4}$ s (where we used the typical values $\varepsilon_{SC} \approx 2 \times 10^3$ and $\rho_{SC} \approx 2 \times 10^4$ Ω m) or for the frequency of $f \approx 1/\tau \approx 10^3$ Hz. When the charges move to the outer SC–air interface, the average separation between the charges located on the glass surface and the outer SC decreases, and in order for the electric potential difference to remain constant, the electric field strength and hence the electroadhesion must increase as the frequency decreases as shown in Fig. 19(a).

Some experiments indicate that as the frequency decreases the electroadhesion force decreases (see Fig. 19(b)). This effect was observed by Meyer *et al.*[1] and may result from a drift of charges from the outer SC to the surface of the touchscreen [this effect depends on the surface and bulk electrical conductivities of the glass], which results in a reduction in the electroadhesion as in Fig. 19(b) (see also Fig. 20). The transfer of charges from the outer SC to the surface of the touchscreen could be strongly affected by ion drift motion in fluid (sweat) and capillary bridges formed between the finger skin and the touchscreen.

In the theoretical calculations, we took the SC Young's modulus $E_{SC} = 40$ MPa, which corresponds to semi-wet skin. If a modulus value less than 40 MPa was taken, the electroadhesion would be larger. This could explain the fluctuations in the measured μ_{on}/μ_{off} typically observed in experimental measurements.

6 Discussion

While the technology for generating tactile feedback on a touchscreen *via* electrovibration (*i.e.* electroadhesion under an oscillating electric field) is already in place and straightforward to implement, our knowledge on contact mechanics for electroadhesion is highly limited. In particular, we still do not know the exact mechanism leading to an increase in tangential frictional forces under electroadhesion. In order to better understand the contact mechanism between the finger pad and touchscreen under electrovibration, we investigated the sliding friction as a function of normal force and the voltage applied to a touchscreen by means of a mean-field theory (Section 4) and experiments performed using a custom-made tribometer (Section 5). Some aspects of these three topics are further discussed in the following subsections.

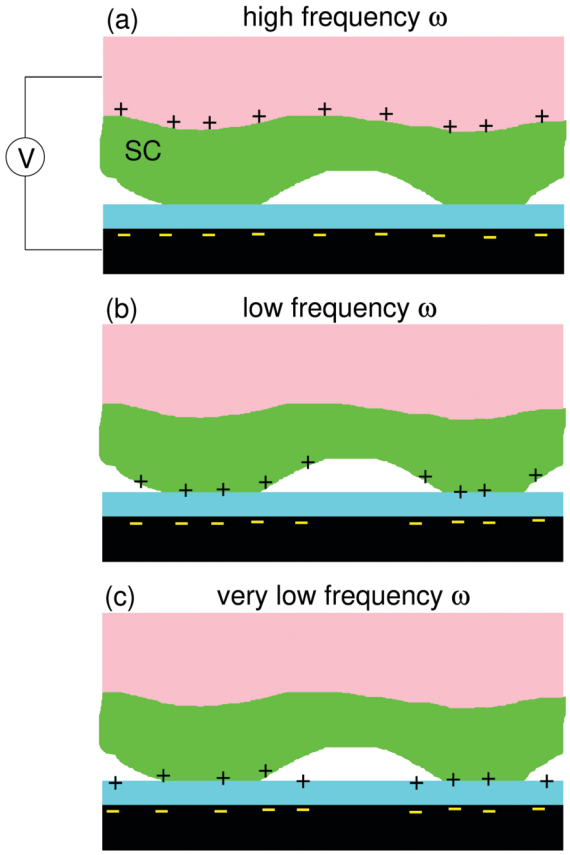

Fig. 20 Distribution of charges at the contact between the skin (green and pink) and a touchscreen (black and blue) when an oscillating electric potential $\phi = V_0\cos(\omega t)$ acts between the skin and the touchscreen. The SC of the skin (green) has a finite electrical conductivity. (a) When the frequency ω is very high, there is not enough time for charges to drift through the SC during the time period of an oscillation $T = 2\pi/\omega$. (b) As ω decreases, charges can drift to the outer surface of the SC. If the electrical resistance of the surface of the touchscreen is infinite, no charges can flow to it. (c) However, the surface of the touchscreen has a finite surface conductivity, and if the frequency ω is small enough, the charges will drift to the surface of the touchscreen, which will reduce the electroadhesive force between the finger and the touchscreen to nearly zero.

Fig. 21 Optical picture taken 500 s after a cylindrical shaped indentor with a diameter of $\approx$3 μm and a wall thickness of $\approx$0.5 μm was pressed into the human wrist skin for $\approx$3 s with a nominal contact pressure of $p_0 \approx 1$ MPa.

6.1 Skin model

Human skin is a multilayer composite material characterized by non-homogeneous, anisotropic, and non-linear properties, and with surface roughness extending over many decades in length scale. In our model, it is assumed that the layer below the SC exhibits uniform mechanical properties and is treated as a linear elastoplastic material. In fact, even a linear viscoelastic model cannot fully describe the response of the skin to external forces. For a linear viscoelastic solid, if an indentor is pressed into its surface for some time period t_0, then the deformations will disappear after a time period of similar order once the indentor is removed. It is easy to test that this is not the case for human skin: Fig. 21 shows an optical picture taken $\approx$10 minutes after a cylinder shaped indentor with a diameter of $\approx$3 mm and a wall thickness of $\approx$0.5 mm was pressed into the human wrist skin for $\approx$3 s with a nominal contact pressure of $p_0 \approx 1$ MPa. The existence of deformations observed even after 10 minutes may be due to the fluid motion in a poroelastic matrix, which cannot be described accurately using a linear viscoelastic model.[52,53]

It is well-known that the friction coefficient of human skin depends on many factors: (1) the material and physical properties of the skin such as the Young's modulus, thickness of the layers, roughness and skin moisture level; (2) physiological conditions of the skin (*e.g.*, age, gender, and ethnicity); (3) environmental conditions (*e.g.*, temperature, humidity); (4) mechanical contact parameters (*e.g.*, anatomical contact region, loading type, direction, speed and magnitude); and (5) contact interface properties (*e.g.*, topologically applied substances and lubrication).[48,54] In this paper, we demonstrated that for a touchscreen providing electrostatic haptic feedback the thickness and dielectric constant of the insulating layer of the touchscreen and the potential difference between the conducting layers also affect the sliding friction. Our numerical results reported in Section 4 demonstrate the effects of the roughness, Young's modulus (E_{SC}), thickness of the SC (d_2), effective thickness of the insulating layers (h_0), and applied nominal contact pressure (p_0). Now, let us discuss and justify the parameters we used in these simulations.

6.1.1 Young's modulus E_{SC} of the SC. Naturally, the skin has three functional layers: epidermis (top layer), dermis (middle layer) and subcutis (bottom layer). The material properties of each layer also depend on many factors (*e.g.*, the anatomy of the skin of an individual person, skin hydration, and the measurement method). Several studies have reported the elastic modulus of the SC (the outermost electrically insulating layer of the epidermis), dermis and subcutis in the ranges of 10 kPa–1 GPa, 0.5 kPa–45 MPa, and 0.12–30 kPa, respectively.[39–41] The mechanical properties are strongly dependent on the environmental conditions: a decrease in the elastic modulus was observed with an increase in either relative humidity or temperature. Papir *et al.*[47] observed that the elasticity of the SC decreases from 8.87 GPa at 26% RH to 2.44 GPa at 68% RH, and an order of magnitude decrease (12 MPa) was observed at 100% RH.

In our model, we assumed that the skin has only two layers: the top layer (SC) and the bulk layer: we varied the Young's modulus of the SC in the range of E_{SC} = 1 MPa–1 GPa and the thickness of the SC in the range of d_2= 100–400 μm while keeping the elastic modulus of the bulk constant (E_{bulk} = 10 kPa).

6.1.2 Power spectrum $C(q)$. Derler *et al.*[54] examined the friction coefficient of dry skin (the index finger and the edge of the hand) against smooth (rms roughness ξ = 0.004 μm) and rough (ξ = 2 μm) glass, and showed that smoother surfaces have higher friction values than rough surfaces. Hendriks and Franklin[55] further showed that the surface roughness of the indenting probe has a dominant effect on the friction coefficient: the smoother the probe surface, the higher the friction coefficient. This result can be explained by the increase in the contact area that would be observed at smoother roughness. On the other hand, for very rough surfaces, Tomlinson *et al.*[56] observed an increasing trend of the friction coefficient for a human finger with increasing material roughness (ξ = 1–25 μm) and then a plateau (ξ = 25–90 μm) for aluminum, brass, and steel. These results show two friction regimes for dry skin with increasing roughness: (1) the friction coefficient initially decreases due to the high real contact area at lower counter surface roughness and then (2) it increases until it reaches a steady state regime due to hysteresis, ploughing, and interlocking.[38] In our model (see Fig. 1), we assume a flat rigid solid surface for the counter surface and hence our findings in Fig. 11 are in an agreement with the first friction regime.

Persson *et al.*[30] measured the surface topography of dry human wrist skin using an optical method with a lateral resolution of 1 μm. Later, Kovalev *et al.*[31] performed AFM measurements at a higher resolution, and combined their measurements with the optical measurements reported in the previous study. Hence, they obtained a surface roughness power spectrum covering over all relevant length scales and reported the rms roughness of the dry human skin as 22 μm. In our work, we adopted the surface roughness power spectrum of the dry human skin from these studies, and also used 4 times higher and lower power spectra in magnitude to consider subject-based variations. Overall, the surface spectrum roughnesses used in the numerical simulations were in agreement with those reported in the literature.

6.1.3 Thickness d_2 of the SC. The thickness of the SC of seven human subjects was determined to vary between 210 and 640 μm by measuring the distance between the skin surface and the border of the living epidermis using optical coherence tomography,[48] while the thickness of an isolated SC was measured to vary between 10 and 40 μm in some other studies.[40,41] In the current study, we assumed that the skin has two layers: the top layer (SC) and the bulk below, and we varied the thickness of the SC in the range of d_2 = 100–400 μm in our model.

6.1.4 Effective thickness h_0 of the insulating layer. The dielectric constant of the insulating layer of the skin is highly dependent on the subject;[47] therefore, we assumed that the effective insulator thickness is in the range of h_0 = 0.1–1 μm to take these variations in the skin related parameters (d_2 and ε_2) into the account. Derler *et al.*[38] measured the surface roughness (R_a) of index finger skin to vary in the range of 6.8–43 μm using a mechanical profilometer (Mahr, Perthometer M1). To our knowledge, no study has been performed to investigate the effect of the thickness of the SC on the sliding friction of skin. Fig. 13 shows the dependency of the SC thickness (d_2) on the relative contact area (A/A_0). Practically, we know that some users of touchscreens experience difficulties in sensing electroadhesion, while some do not. This might be due to the thickened SC regions formed as a result of pressure and repeated wear, which leads to a lower relative contact area, and hence lower frictional force under electroadhesion. Also, the findings given in Fig. 14 are very important and show that the normalized contact area and hence the frictional force can be increased significantly by modifying the effective thickness of the insulating layer of the touchscreen. Based on our assumptions in this study, it appears that the thickness of the insulating film on the substrate has the largest contribution to h_0, and it is possible to reduce h_0 down to $\approx$0.1 μm for achieving a stronger tactile effect.

6.1.5 Applied nominal contact pressure p_0. The measured friction coefficient of the skin is strongly dependent on the applied normal load. In the literature,[38,42] it has been reported that the contact area and hence the friction force increase as the normal load applied by the human finger is increased. This result matches with our findings shown in Fig. 15.

6.1.6 Frictional shear stress τ_f. Estimating the frictional shear stress τ_f acting in the contact regions between a human finger and a touchscreen is difficult since it depends on contamination films (*e.g.*, oil and water on the finger) and their composition and spatial distribution, which are not known in detail and vary from one individual to the next. We note, however, that the value used for frictional shear stress in our theoretical calculations is very close to what has been measured in earlier experimental studies on human finger–glass interaction under sliding.[30,31]

Unfortunately, the theoretical calculation of frictional shear stress under the conditions of boundary lubrication is a highly challenging task. Even in the most idealized situation with perfectly smooth surfaces, no contamination films, and the exact knowledge about the atomic positions, it is almost impossible to accurately calculate the frictional shear stress using even a first principles theory like density functional theory (or the less first-principles approach of molecular dynamics).

6.2 Tactile perception of electrovibration

One interesting observation is that the electroadhesion between a finger and a touchscreen can be felt only indirectly as a change (increase) in the sliding friction force. That is, when a stationary finger is gently pressed on the touchscreen, the electrovibration cannot be perceived. The reason for this is as follows: when a voltage is applied to the conductive layer of a touchscreen, an attractive stress will act on the skin in non-contact areas. The increase in total attractive force due to electroadhesion will be compensated for by an increase in the repulsive force and the magnitude of the total normal force acting on the finger (and on the touchscreen) will remain unaltered (and equal to the applied normal force).

Blood and lymphatic vessels as well as most nerves and sensory receptors (for pain, pressure, touch, *etc.*) are located in the dermis. However, since most of the electrovibration induced deformations in the skin are localized to the SC, the mechanoreceptors do not experience any stress to stimulate the spiking and convey information through nerve fibers to the brain. As a result, the electrovibration cannot be perceived when the finger is stationary. For sliding contact, instead, an additional friction force develops due to the change in real contact area between the finger and the touchscreen, which results in a fluctuating shear deformation on the finger. Hence, the Pacinian corpuscles (FA II receptors) which are sensitive to vibrations at frequencies varying between 5 and 500 Hz (the main frequency of the friction signal was 250 Hz in our system, see Fig. 10) will be deformed and emit neural signals.[57] The discussion reported by Vardar *et al.*[19] is in agreement with our arguments given above where they suggested that a Pacinian corpuscle is the primary psychophysical channel in the detection of the electrovibration stimuli.

7 Limitations of the study and further research questions

In this study, we have assumed that the only attraction between the finger and the touchscreen is the electrostatic force originating from the applied potential. In reality, there will always be other attractive interactions between two contacting solids: for example, the van der Waals interaction will operate between all solids and capillary bridges can be very important for human skin. These additional interactions can be included in future studies. For example, the role of capillary bridges in adhesion was previously studied,[21] and a more general theory of adhesion was developed.[22,58]

In the theory presented above, we have neglected electrical breakdown across the narrow gap between the contacting solids.[59] When a large electric potential is applied between narrowly separated surfaces, a very large electric field can prevail, in particular close to high and sharp asperities. If the local electric field becomes larger than some critical value, breakdown occurs. For gap separations of ≈ 1 μm or less, which is typical in many applications, the breakdown voltage is typically a few hundred volts.

Furthermore, the reason for the discrepancies between the experiments and theory shown in Fig. 17 might be due to the variations in the angle of contact made by the finger with the touchscreen during the measurements, and changes in the hydration level of the skin due to the sweat and sebum excretion to the contact interface, which are highly challenging to control during the measurements.[60]

8 Conclusions

We have studied the contact mechanics between the human finger and a touchscreen when an electric potential exists between them. We have presented a detailed theoretical study of how the area of real contact and the friction force depend on contact parameters such as the nominal contact pressure and the applied voltage. For example, we show that when the Young's modulus of the SC is reduced due to finger moisture or an increase in relative humidity in the environment, the separation between the finger and the touchscreen decreases, and hence the real contact area increases, which results in higher frictional forces acting on the finger during sliding. Our study shows that it is possible to increase the friction force by using a thinner insulating film on the touchscreen. We have also presented experimental data for how the friction force depends on the applied normal load and on the potential difference between the finger and the touchscreen. The experimental results were compared with the predictions made by the proposed theory, and a good agreement was observed. Finally, the dependency of the electroadhesion friction on the frequency of the oscillating electric potential has been investigated by using the proposed model and the results were compared with the recent experimental data reported in the literature.

Conflicts of interest

There are no conflicts to declare.

Appendix A

Plastic deformation and finite-size effects

When solids with large elastic moduli and large surface roughnesses are squeezed into contact, the local pressure in asperity contact regions becomes so high that the softer material yields plastically. When the nominal contact pressure is small, the solids make contact in only a few macroasperity contact regions. In this case, one needs to take into account what we refer to as finite-size effects when calculating the distribution of interfacial separation. In this section, we will show that both these effects are important for the contact between the human dry skin and a hard counter surface.

The elastic modulus of the SC depends on the relative humidity or wetness of the skin. Thus, dry skin has a Young's modulus of the order of $E \approx 1$ GPa, as typical for glassy polymers. When the humidity increases, E decreases, such that at 100% relative humidity (wet state) $E \approx 10$ MPa. The drop in the modulus with increasing humidity is due to the swelling and break-up of weak bonds (*e.g.*, hydrogen bonds) in the skin by the water molecules, which lower the energetic barriers for rearranging segments of the polymer chains. This effectively converts the SC from a stiff glassy material to a soft rubbery material.

The drop in the Young's modulus of skin with increasing humidity is similar to the influence of temperature on the viscoelastic modulus of rubber. At low temperatures (corresponding to dry skin) rubber is in the glassy state with a Young's

modulus of the order of $E \approx 1$ GPa. At high temperatures (corresponding to wet skin), it is in the rubbery state where the Young's modulus is in the order of a few MPa.

Plastic deformation

Consider the contact between human skin and a hard counter surface. When the elastic modulus of the SC is below $\sim$100 MPa, the contact pressures are typically below 50 MPa and we will assume that no plastic deformations occur on the SC. However, for dry skin, $E > 1$ GPa, the stress in the asperity contact regions will be so high as to result in plastic deformation of the SC.

If an indentor is pushed into a linear viscoelastic solid for a certain period of time t_0, and then removed, the deformation will disappear after a time period of the order of t_0. This is not observed for the human SC where the deformations need a longer time to disappear. This is similar to plastic deformation, but in contrast to plastic deformation of crystalline solids (*e.g.* metals), the deformation of the SC will slowly disappear after the external force field is removed. A more accurate model for the SC is a non-linear viscoelastic model of the following type: we assume that the external force pushes molecular groups (here polymer segments) over energetic barriers which are so large that thermal fluctuations require a very long time to "move" the molecular groups back to the original minimum free-energy state (here the undeformed state). This effect is well known for rubber materials below the glass transition temperature where plastic deformations induced by external forces will not disappear when the force field is removed even after a very long waiting time. However, if the rubber is warmed up to room temperature, relaxation occurs and deformations rapidly disappear.[43] This shows that no strong covalent bonds break in the rubber during the deformations, as this would result in permanent (irreversible) changes in the molecular arrangements. Instead, the external forces move molecular segments from one position to another, and the energetic barriers separating the different geometrical arrangements of the polymer segments are too high to be overcome by thermal fluctuations at low temperatures, resulting in an apparent permanent plastic deformation of the rubber.

For the contact between elastoplastic solids, the concept of magnification is very important. When the interface is observed at the magnification ζ, only roughness with wavenumber $q < \zeta q_0$ is observed, where q_0 is the smallest wavenumber. If the contact pressure in the asperity contact regions observed at the magnification ζ is below the penetration hardness σ_Y, the solids deform elastically. However, when we increase the magnification, we observe more surface roughness at shorter length scales and the contact area decreases. As a result, the contact pressure in the asperity contact regions increases as ζ increases. Finally, the contact pressure may be so high as to plastically deform the solid at short length scales.

When the compressive force is removed, the deformations on long length scales, which were elastic, will disappear. However, the short length scale deformations in the asperity contact regions by plastic flow will remain and effectively smooth out the solid surfaces in the asperity contact regions at short length scales. If the solids are compressed to make contact for the second time with the same normal force F_N as in the first contact, the solids deform purely elastically and the contact area can be obtained using the surface roughness power spectrum $C_{pl}(q)$ of the (plastically) deformed surface. It was shown that C_{pl} can be obtained approximately using (with $\zeta = q/q_0$)

$$C_{pl}(q) = \left(1 - \left(\frac{A_{pl}(\zeta)}{A_{pl}^o}\right)^6\right) C(q) \qquad (28)$$

where $A_{pl}^o = F_0/\sigma_Y$ (F_0 is the normal load) is the contact area, assuming that all contact regions have yielded plastically so the pressure in all contact regions is equal to the penetration hardness.[61,62] The basic picture behind this definition is that surface roughness at short length scales gets smoothed out by plastic deformation, resulting in an effective cut-off of the power spectrum for large wave vectors (corresponding to short distances). The blue curve in Fig. 5 was obtained by using (28).

We now show numerical results illustrating the role of plastic deformations for dry skin. Fig. 22 shows the normalized contact area A/A_0 as a function of the magnification $\zeta = q/q_0$ (log–log scale) for $E_{SC} = 1$ GPa and assuming the penetration hardness $\sigma_Y = 50$ MPa.[25] We have assumed the thickness of the SC to be $d_2 = 200$ μm, and that the skin below the SC has a Young's modulus E_{bulk} of 10 kPa. The red curve shows the asperity contact area which is elastically deformed, and the green curve represents the area which is plastically deformed. The blue curve is the elastic contact area during the second contact with the plastically smoothed surface having the power spectrum given by the blue curve in Fig. 5.

Fig. 22 shows that assuming elastic contact and using the power spectrum (28) result in virtually the same contact area (numerically), as a function of magnification, as predicted for the original surface using the elastoplastic contact mechanics theory, where $A(\zeta) = A_{el}(\zeta) + A_{pl}(\zeta)$.

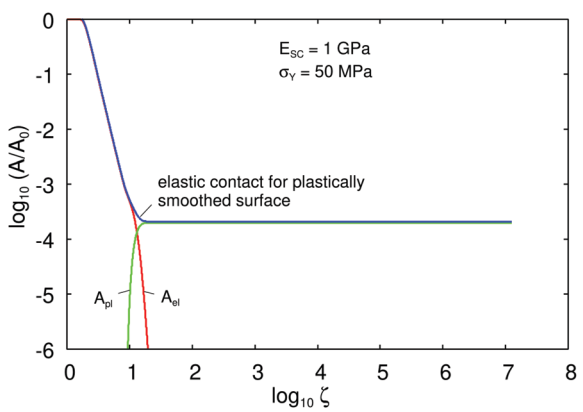

Fig. 22 The normalized contact area A/A_0 as a function of the magnification $\zeta = q/q_0$ (log–log scale) for $E_{SC} = 1$ GPa, $\sigma_Y = 50$ MPa, $d_2 = 200$ μm, and $E_{bulk} = 10$ kPa. The red curve is for the asperity contact area which is elastically deformed and the green curve is for the area which is plastically deformed. The blue curve is for the elastic contact area during the second contact with the plastically smoothed surface having the power spectrum given by the blue curve in Fig. 5.

Finite size effects

Next, let us discuss what we refer to as finite size effects. Infinite solids with randomly rough surfaces have infinitely high asperities. In fact, such solids have a Gaussian height probability distribution, with a tail extending to infinite height. Analytical contact mechanics theories implicitly assume infinitely large surfaces and will therefore have infinitely many high asperities. However, real solids are finite and will always have the highest asperity, and when the separation between two solids is large enough, no contact will occur between the solids.

As long as the force squeezing two elastic solids together is large enough, many macroasperity contacts will occur, if, at least, the roughness power spectrum of one of the surfaces has a long wavelength roll-off region, as is the case for most surfaces of interest such as human skin. In that case, the contact mechanics for a finite and an infinite system, with randomly rough surfaces having the same statistical properties, will be nearly the same. However, for small applied normal force, this is not the case, and we refer to this as the finite-size effect. Here, we note that the relation between the applied nominal contact pressure and the average surface separation is very different when the squeezing pressure is in the finite size regime, as compared to higher squeezing pressures. This topic has been already studied in depth,[24,53] and here we only show numerical results relevant to human skin.

Fig. 23 shows the logarithm of the nominal contact pressure p_0 as a function of the average interfacial separation $\bar{u}$ for E_{SC} = 40 MPa (semi-wet skin). The solid line is for an infinite, randomly rough surface (which has infinitely many high asperities), while the dashed line is for a finite system with q_0 = 800 m^{-1} corresponding to the length scale $L = 2\pi/q_0 \approx 1$ cm, which is a typical diameter for the apparent contact area between a fingerpad and a touchscreen. In the calculations, we have used the red-colored power spectrum shown in Fig. 5 and assumed d = 200 μm and E_{bulk} = 10 kPa. Note that the finite-size effects are important when $p_0 < p_c$, where $p_c \approx 10^4$ Pa.

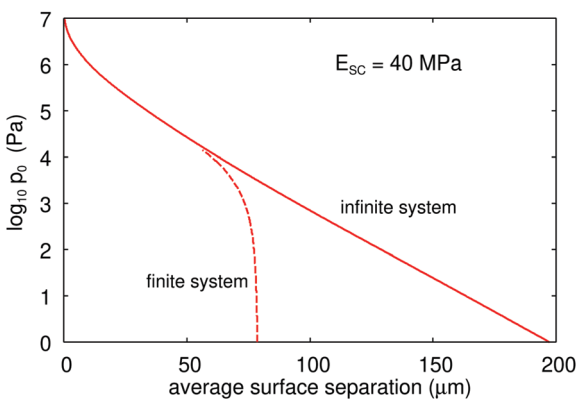

Fig. 23 The logarithm of the nominal contact pressure p_0 as a function of the average interfacial separation $\bar{u}$ for E_{SC} = 40 MPa. The solid curve is for an infinite, randomly rough, surface (which has infinite high asperities), while the dashed curve is for a finite system with q_0 = 800 m^{-1} corresponding to the length $L = 2\pi/q_0 \approx 1$ cm. In the calculations, we have used the red-colored power spectrum shown in Fig. 5 with d_2 = 200 μm and E_{bulk} = 10 kPa. Note that finite-size effects are important when $p_0 < p_c$ where $p_c \approx 10^4$ Pa.

In this paper, we have included the finite size effects in the following way: since $\bar{u}$ changes rather slowly with the contact pressure for $p_0 < p_c$ (see the dashed line in Fig. 23) we use the same probability distribution of interfacial separations obtained for $p = p_c$ (as given by the Persson contact mechanics theory). This approach ignores the increase in the surface separation observed when p_0 decreases below p_c (see the dashed line in Fig. 23).

Acknowledgements

This work was performed within a Reinhart-Koselleck project funded by the Deutsche Forschungsgemeinschaft (DFG). BNJP would like to thank DFG for the project support under the reference German Research Foundation DFG-Grant: MU 1225/36-1. MA acknowledges FZ-Jülich for the support and the kind hospitality received during their visit to PGI-1, where most of this work was performed. OS acknowledges the doctoral fellowship support provided by TUBITAK under the BIDEB-2211 program. CB acknowledges the financial support provided by TUBITAK under the contract number 117E954. Finally, the authors are grateful to Dr Ozgur Birer from Koc University for the FESEM micrographs.

Notes and references

1 D. J. Meyer, M. A. Peshkin and J. E. Colgate, *World Haptics Conference (WHC)*, 2013, pp. 43–48.
2 C. Xu, A. Israr, I. Poupyrev, O. Bau and C. Harrison, *CHI'11 Extended Abstracts on Human Factors in Computing Systems*, 2011, pp. 317–322.
3 H. Tang and D. J. Beebe, *IEEE Trans. Rehabil. Eng.*, 1998, **6**, 241–248.
4 S.-C. Kim, A. Israr and I. Poupyrev, *Proceedings of the 26th Annual ACM Symposium on User Interface Software and Technology*, 2013, pp. 531–538.
5 D. Wijekoon, M. E. Cecchinato, E. Hoggan and J. Linjama, *International Conference on Human Haptic Sensing and Touch Enabled Computer Applications*, 2012, pp. 613–624.
6 M. Wiertlewski, R. F. Friesen and J. E. Colgate, *Proc. Natl. Acad. Sci. U. S. A.*, 2016, **113**, 9210–9215.
7 M. K. Saleem, C. Yilmaz and C. Basdogan, *IEEE Trans. Haptics*, 2018, **11**, 599–610.
8 A. Johnsen and K. Rahbek, *J. Inst. Electr. Eng.*, 1923, **61**, 713–725.
9 E. Mallinckrodt, A. Hughes and W. Sleator Jr, *Science*, 1953, **118**, 277–278.
10 T. Nakamura and A. Yamamoto, *ROBOMECH J.*, 2017, **4**, 18.
11 J. Shintake, S. Rosset, B. Schubert, D. Floreano and H. Shea, *Adv. Mater.*, 2016, **28**, 231–238.
12 G. Monkman, *Ind. Robot*, 2003, **30**, 326–330.
13 R. M. Strong and D. E. Troxel, *IEEE Transactions on Man-Machine Systems*, 1970, **11**, 72–79.

14 C. D. Shultz, M. A. Peshkin and J. E. Colgate, *World Haptics Conference (WHC), 2015 IEEE*, 2015, pp. 57–62.
15 S. Grimnes, *Acta Physiol.*, 1983, **118**, 19–25.
16 B. N. J. Persson, *Sliding Friction: Physical Principles and Applications*, Springer, Heidelberg, 2000.
17 E. Gnecco and E. Meyer, *Elements of Friction Theory and Nanotribology*, Cambridge University Press, 2015.
18 J. N. Israelachvili, *Intermolecular and Surface Forces*, Academic Press, 2011.
19 Y. Vardar, B. Güçlü and C. Basdogan, *IEEE Trans. Haptics*, 2017, **10**, 488–499.
20 B. N. J. Persson, *J. Chem. Phys.*, 2018, **148**, 144701.
21 B. N. J. Persson, *J. Phys.: Condens. Matter*, 2008, **20**, 315007.
22 B. N. J. Persson and M. Scaraggi, *J. Chem. Phys.*, 2014, **141**, 124701.
23 A. Almqvist, C. Campaná, N. Prodanov and B. N. J. Persson, *J. Mech. Phys. Solids*, 2011, **59**, 2355–2369.
24 L. Afferrante, F. Bottiglione, C. Putignano, B. N. J. Persson and G. Carbone, *Tribol. Lett.*, 2018, **66**, 75.
25 B. N. J. Persson, *J. Chem. Phys.*, 2001, **115**, 3840–3861.
26 B. N. J. Persson, *J. Phys.: Condens. Matter*, 2012, **24**, 095008.
27 A. Chateauminois and C. Fretigny, *Eur. Phys. J. E: Soft Matter Biol. Phys.*, 2008, **27**, 221.
28 K. G. Rowe, A. I. Bennett, B. A. Krick and W. G. Sawyer, *Tribol. Int.*, 2013, **62**, 208–214.
29 B. Lorenz, Y. Oh, S. K. Nam, S. H. Jeon and B. N. J. Persson, *J. Chem. Phys.*, 2015, **142**, 194701.
30 B. N. J. Persson, A. Kovalev and S. N. Gorb, *Tribol. Lett.*, 2013, **50**, 17–30.
31 A. E. Kovalev, K. Dening, B. N. J. Persson and S. N. Gorb, *Beilstein J. Nanotechnol.*, 2014, **5**, 1341.
32 P. G. Whitten and H. R. Brown, *Phys. Rev. E: Stat., Nonlinear, Soft Matter Phys.*, 2007, **76**, 026101.
33 T. Vodlak, Z. Vidrih, E. Vezzoli, B. Lemaire-Semail and D. Peric, *Biotribology*, 2016, **8**, 12–25.
34 T. Yamamoto and Y. Yamamoto, *Med. Biol. Eng.*, 1976, **14**, 494–500.
35 B. M. Dzidek, M. J. Adams, J. W. Andrews, Z. Zhang and S. A. Johnson, *J. R. Soc., Interface*, 2017, **14**, 20160935.
36 S. Bochereau, B. Dzidek, M. Adams and V. Hayward, *IEEE Trans. Haptics*, 2017, **10**, 456–465.
37 H. Fruhstorfer, U. Abel, C.-D. Garthe and A. Knüttel, *Clin. Anat.*, 2000, **13**, 429–433.
38 S. Derler, L.-C. Gerhardt, A. Lenz, E. Bertaux and M. Hadad, *Tribol. Int.*, 2009, **42**, 1565–1574.
39 Y. Yuan and R. Verma, *Colloids Surf., B*, 2006, **48**, 6–12.
40 C. Pailler-Mattei, S. Pavan, R. Vargiolu, F. Pirot, F. Falson and H. Zahouani, *Wear*, 2007, **263**, 1038–1043.
41 M. Geerligs, L. Van Breemen, G. Peters, P. Ackermans, F. Baaijens and C. Oomens, *J. Biomech.*, 2011, **44**, 1176–1181.
42 M. J. Adams, B. J. Briscoe and S. A. Johnson, *Tribol. Lett.*, 2007, **26**, 239–253.
43 A. Tiwari, N. Miyashita, N. Espallargas and B. N. J. Persson, *J. Chem. Phys.*, 2018, **148**, 224701.
44 P. R. Gray, P. Hurst, R. G. Meyer and S. Lewis, *Analysis and Design of Analog Integrated Circuits*, Wiley, 2001.
45 C. Hsieh, H. Jain and E. Kamitsos, *J. Appl. Phys.*, 1996, **80**, 1704–1712.
46 D. Fischer, *Fujitsu Microelectronics Europe*, 2010.
47 Y. S. Papir, K.-H. Hsu and R. H. Wildnauer, *Biochim. Biophys. Acta, Gen. Subj.*, 1975, **399**, 170–180.
48 X. Liu, PhD thesis, University of Sheffield, 2013.
49 M. Ayyildiz, M. Scaraggi, O. Sirin, C. Basdogan and B. N. J. Persson, *Proc. Natl. Acad. Sci.*, 2018, **115**, 12668–12673.
50 B. Delhaye, P. Lefevre and J.-L. Thonnard, *J. R. Soc., Interface*, 2014, **11**, 20140698.
51 C. Shultz, E. Colgate and M. A. Peshkin, *IEEE Trans. Haptics*, 2018, **11**, 279–290.
52 R. Oftadeh, B. K. Connizzo, H. T. Nia, C. Ortiz and A. J. Grodzinsky, *Acta Biomater.*, 2018, **70**, 249–259.
53 L. Pastewka, N. Prodanov, B. Lorenz, M. H. Müser, M. O. Robbins and B. N. J. Persson, *Phys. Rev. E: Stat., Nonlinear, Soft Matter Phys.*, 2013, **87**, 062809.
54 S. Derler and L.-C. Gerhardt, *Tribol. Lett.*, 2012, **45**, 1–27.
55 C. Hendriks and S. Franklin, *Tribol. Lett.*, 2010, **37**, 361–373.
56 S. Tomlinson, R. Lewis and M. Carré, *Wear*, 2009, **267**, 1311–1318.
57 H. P. Saal, B. P. Delhaye, B. C. Rayhaun and S. J. Bensmaia, *Proc. Natl. Acad. Sci. U. S. A.*, 2017, **114**, E5693–E5702.
58 B. N. J. Persson, *Eur. Phys. J. E: Soft Matter Biol. Phys.*, 2002, **8**, 385–401.
59 F. W. Strong, J. L. Skinner, P. M. Dentinger and N. C. Tien, *Reliability, Packaging, Testing, and Characterization of MEMS/MOEMS V*, 2006, p. 611103.
60 T. André, V. Lévesque, V. Hayward, P. Lefèvre and J.-L. Thonnard, *J. R. Soc., Interface*, 2011, **8**, 1574–1583.
61 B. N. J. Persson, B. Lorenz and A. Volokitin, *Eur. Phys. J. E: Soft Matter Biol. Phys.*, 2010, **31**, 3–24.
62 B. N. J. Persson, *Tribol. Lett.*, 2016, **63**, 42.